Kinetic and fluid dynamic modeling of ethylene jet flames in diluted and heated oxidant stream combustion conditions

Seyed Reza Shabanian[1,3], Paul Ross Medwell[2], Masoud Rahimi[*,1], Alessio Frassoldati[,3], Alberto Cuoci[3]**

[*]masoudrahimi@yahoo.com; [**]alessio.frassoldati@polimi.it

1-CFD Research Center, Chemical Engineering Department, Razi University, Kermanshah, Iran

2-School of Mechanical Engineering, The University of Adelaide, South Australia 5005, Australia

3-Politecnico di Milano, Dipartimento di Chimica, Materiali e Ingegneria Chimica "G. Natta", Milano, Italy

Abstract

This paper reports the results of a numerical investigation of several turbulent nonpremixed ethylene jet flames, either undiluted or diluted with hydrogen, air or nitrogen, which have been experimentally studied using a jet in hot coflow (JHC) burner. The fuel jet issues into a hot and highly diluted coflow at two O_2 levels (3% or 9%) and a temperature of 1100 K. These conditions emulate those of moderate or intense low oxygen dilution (MILD) combustion. The attention is mainly focused on assessing the performance of different models for the turbulence–chemistry interaction. The model predictions are compared to experimental measurements. The eddy dissipation concept (EDC), flamelet and PDF transport models were used in combination with a two-equation turbulence model (k-ε) and two different kinetic mechanisms (GRI-Mech 3.0 and POLIMI). The effect of the oxygen concentration in the coflow is well captured by all models. A modified version of the EDC model, recently proposed for the modeling of methane MILD combustion conditions, is also used. This model significantly improves the predictions of the EDC in the case of the ethylene flames studied in this paper. The agreement between measurements and predictions of the flamelet model is generally not as good as the PDF transport and modified EDC models, whose predictions are in good agreement with the measurements, and are improved especially for the apparent liftoff heights and the peak flame temperature. The effect of the fuel composition on the CH_2O formation is also discussed, showing generally good agreement.

Abbreviated Title: CFD and kinetic modeling of ethylene jet flames

Keywords: MILD combustion, flameless combustion, jet in hot coflow burner, turbulence–chemistry interaction.

1. Introduction

Increasing energy demand and the concerns surrounding combustion generated pollution requires new combustion technologies to be sought that are more efficient and environmentally sustainable. MILD (moderate or intense low oxygen dilution) combustion [1] is an innovative technique which offers a possible solution to this problem as it allows a simultaneous enhancement in thermal efficiency of combustion systems and lower pollutant emissions. This combustion regime proceeds in an environment of low oxygen concentration at high oxidizer temperatures to create a more uniform and distributed combustion region which gives higher efficiency, radiation flux and lower levels of pollutants. As a result, the combustion process takes place in a more diluted fashion and thus the temperature peaks that are largely responsible for NO_x formation can be avoided. In comparison with conventional combustion regimes, MILD combustion has been reported to provide energy savings of approximately 30%, a 30% reduction in furnace size and a 25% reduction in pollutant emissions [2].

Wünning and Wünning [3] showed MILD combustion (also referred to as flameless oxidation, FLOX®) to be highly efficient with low NO_x emissions. There have been numerous MILD combustion studies in semi-industrial scale furnaces [4,5] and burners [6,7,8], both experimentally and using mathematical modeling based on the eddy dissipation concept (EDC) [9,10] and conditional moment closure (CMC) [11]. Danon and coworkers recently studied a multi-burner flameless combustion furnace. They first studied experimentally [12] the effect of the position of the burners and found the optimal operating conditions. Then, they performed numerical simulations using the EDC model to achieve more insight regarding the effects of burner positioning in their multi-burner flameless combustion furnace [13].

A review of the research efforts in modeling MILD combustion have been presented by Aminian *et al.* [14] and De *et al.* [15]. These authors also discussed the applicability of the eddy dissipation concept to the modeling of jet in hot coflow (JHC) flames and proposed a modified EDC model capable of enhancing the predictions of mean temperature field in JHC conditions. The interest in the JHC burner is motivated by its ability to emulate MILD combustion under controlled conditions.

Previous studies have mainly concentrated on the combustion of CH_4 or CH_4/H_2 mixtures, while in this study the focus is on the modeling of ethylene (C_2H_4) flames. The interest toward ethylene is motivated by the significance of this species as an important intermediate in the oxidation of larger hydrocarbons, and also to bridge the gap between methane and the more complex chemistry of practical fuels. In order to advance fundamental understanding of MILD combustion, Medwell *et al.* [16] studied the combustion of $C_2H_4/H_2/O_2/N_2$ mixtures in the JHC burner of the University of Adelaide. In the current work we

discuss the results of CFD modeling of the JHC experiments, with particular attention to the effect of the models adopted with a RANS approach for the modeling of turbulence and turbulence–chemistry interactions. In particular, we examine the effects of combustion and turbulence models, differential diffusion and chemical kinetic mechanisms on the accuracy of the predictions.

2. Burner description and computational domain

The burner in this study is the jet in hot coflow (JHC) burner, used previously by Medwell *et al.* [16,17] and is shown in Fig. 1. It consists of a central insulated fuel jet (Ø4.6 mm) within an annular coflow (Ø82 mm) of hot exhaust products from a premixed secondary burner mounted upstream of the jet exit plane. The O_2 level of the coflow is controlled by the secondary porous burner to give O_2 levels of 3 or 9% (volumetric), while the coflow temperature and exit velocity were kept constant at 1100 K and 2.3 m/s. The fuel used in the jet is ethylene (>99% C_2H_4), either undiluted, or diluted with hydrogen (H_2), air, or nitrogen (N_2). A description of the experimental details is provided in ref. [16] and [17].

It is worth noting that although the experimental results presented in the present paper are shown on the graphs only as a line, there are inherent experimental errors and uncertainties. Factors such as correction for the Rayleigh cross-section (for temperature), collisional quenching (for OH), laser power fluctuations, and noise all affect the experimental measurements. Analysis of measurements in a flat-flame indicates systematic errors of 5% and 2.5% for the OH and temperature, respectively. In a turbulent flame these errors are estimated to be less than 20% in the worst case, and for the averaged data presented in this paper less than 10%.

In this work, numerical simulations are performed to model the flames in the JHC burner developed and experimentally studied by Medwell *et al.* [16]. The flames were simulated with the commercial CFD code FLUENT 12.1.4. A two-dimensional steady-state simulation of the physical domain was considered due to the symmetry of the system. Figure 2 shows the computational grid used to simulate the flames and the boundary conditions adopted. The grid domain is 400 mm in the axial direction and 120 mm in the radial direction from the jet exit. It is a structured non-uniform grid with 34,200 cells, which provides high resolution in the reaction zone region and close to the inlets and save computational effort elsewhere. This grid layout was selected based on an examination of different cell sizes, and no further significant change was obtained for finer cells. The flame is non-confined and hence a pressure outlet condition is used (see Fig. 2) assuming ambient air backflow conditions. The simulations were performed for two different O_2 mole fractions in the coflow stream, namely 3% and 9%. Figure 3 anticipates the results of some model predictions which are discussed later. It compares predicted temperature fields and photographs of the

flame [16] and clearly shows the effect of the different amount of oxygen in the oxidizer. Consistent with the 'flameless' characteristics of MILD combustion, the photographs may indicate that the flames appear lifted, but reactions are indeed present between the jet exit plane and the visible flame. The presence of soot at the downstream locations is a result of the entrainment of surrounding air beyond the confines of the coflow, where MILD combustion conditions are no longer maintained. As expected, combustion occurs with weaker or higher intensity according to the oxygen content in the oxidizer stream.

The aim of this work is first to identify key modeling issues for predicting temperature and chemical species in the ethylene JHC experiments and then to discuss the effect of fuel composition on the reactivity of the reacting mixture using two kinetic mechanisms.

3. Modeling

Christo and Dally [9] have shown that in the case of the JHC burner fed with CH_4/H_2, differential diffusion effects have a strong influence on the accuracy of the predictions and that conserved scalar based models, *i.e.* the ξ/PDF and flamelet models (adopting equilibrium or finite rate chemistry), are inadequate for modeling jet in hot coflow (JHC) flames. Moreover, they also discussed the importance of using detailed chemical kinetics, rather than global or simplified mechanisms.

It is important to notice that, compared to traditional diffusion flames, the uniform conditions and low oxygen concentration in MILD combustion regime, leads to slower reaction rates and enhances the influence of molecular diffusion on flame characteristics. These two effects challenge the applicability of simple combustion models that assume fast chemistry and neglect the effects of differential diffusion [9].

The objective of the study reported in this work is to assess the performance of the different turbulence–chemistry interaction models in combination with different turbulence models and chemical kinetic mechanisms in predicting JHC ethylene flames by comparing predictions with experimental data. One of the main differences, compared to the previous methane (and CH_4/H_2) cases, is that ethylene is characterized by a significantly higher reactivity and relatively more complex chemistry. The kinetic model adopted should be able to properly characterize the role of vinyl radicals and the higher acetylene formation in ethylene combustion. Moreover, ethylene has a greater tendency to form soot.

3.1. Turbulence and Radiation models

The burner was modeled using several turbulence and radiation models to simulate the flames. To model turbulence, three different models have been evaluated: the modified standard *k*-ε (modified SKE), the renormalization group (RNG) *k*-ε and the Reynolds Stress model (RSM). The standard *k*-ε model is a semi-empirical approximation based on solving transport equations for the turbulence kinetic energy (*k*) and its dissipation rate (ε), with both equations containing a number of empirical constants. In this model, the flow is assumed fully turbulent, and the effects of molecular viscosity are neglected. Assumption of an isotropic scalar quantity for the turbulent viscosity is another approximation of the standard *k*-ε model. This model is known for its shortcomings in predicting round jets. In particular, the standard *k*-ε model over-predicts the decay rate and the spreading rate of a round jet. The $C_{1\varepsilon}$ parameter is modified to a value of 1.60 for self-similar round jets [18]. The RNG *k*-ε model has a formulation similar to that of the SKE model, although it uses different constants and has additional terms and functions in the transport equations of *k* and ε. In this model, there are exact expressions for the turbulent Prandtl and Schmidt numbers. The RNG model is expected to yield better results in predicting round jets, swirling flows and flows with a recirculation region in comparison with the SKE model [19]. The Reynolds stress model (RSM) involves calculation of the individual Reynolds stresses using differential transport equations. The Navier-Stokes equations with Reynolds stress model become stiff and time consuming in convergence compared to the *k*-ε model. The RSM does not use the Boussinesq hypothesis and isotropic turbulent viscosity assumption. Gran *et al.* [20] have reported improvement in prediction of observed flow patterns in the near burner zone for combusting flows using the RSM.

As suggested by Christo and Dally [9], Frassoldati *et al.* [10], and Aminian *et al.* [14], the discrete ordinate (DO) radiation model [21] has been used to calculate the flame thermal radiation. This model can be used for a wide range of optical thicknesses. The model solves a radiative transfer equation for a number of discrete solid angles across the computational domain. For the model, theta-divisions and phi-divisions define the number of control angles used to discretize each octant of the angular space. Also, theta-pixels and phi-pixels are used to control the pixelation that accounts for any control volume overhang. The model computes the absorption coefficient from the weighted sum of the gray gas model (WSGGM) in which spatial variation in the total emissivity is computed as a function of gas composition and temperature. The WSGGM is a model with reasonable accuracy that takes into account particular absorption bands. It is worth noting that the effects of radiation on the flame are negligible when in the

confines of the hot coflow (axial distance below ~120 mm) (refer to Figure S1 in the supplemental material for further details).

3.2. Turbulent combustion models

The main challenges in modeling turbulent combustion are handling the mean rate of reaction and adequate representation of the chemistry in the model. In this study the capability of three classes of combustion models for predicting MILD flames is assessed: volumetric reaction-based models, conserved scalar based models and PDF transport models. The eddy dissipation concept (EDC) model [22,23] and the modified EDC [15,24] belong to the first category, the Steady Laminar Flamelets (SLF) model [25,26] to the second. Finally, the composition PDF transport models allow simulating finite-rate chemistry in turbulent flames without the assumptions needed to model the unknown terms which arise from the Reynolds-averaging of the energy and species balance equations. Nevertheless, the PDF transport models require the modeling of the molecular mixing of species and heat which is usually the most significant source of error in the PDF transport approach.

3.2.1. Eddy dissipation concept model

The eddy dissipation concept (EDC) model has the advantage of incorporating detailed kinetics at a computational cost which is quite moderate compared to more advanced models such as the transported PDF method, especially if the *in-situ* adaptive tabulation (ISAT) model [27] is used. As already discussed by De *et al.* [15], however, this advantage comes at the cost of a less accurate description of turbulent fluctuations.

In a turbulent environment, combustion takes place where there is a molecular mixing, *i.e.* at small turbulence scales. According to the EDC model, the chemical reactions occur only in small scale micro-mixed turbulent structures known as fine structures.

The evolution of species mass fractions inside the fine scales (ω^*) is then computed by integrating the chemistry within these fine scales for a residence time τ^*.

$$\tau^* = C_\tau \left(\frac{\nu}{\varepsilon}\right)^{1/2} \quad (1)$$

where C_τ is a time scale constant equal to 0.4082 in the standard EDC model and becomes C_τ=3.0 in the modified EDC proposed by De *et al.* [15]. Here ν is the laminar kinematic viscosity.

The size of the fine scales is modeled as a function of the local turbulent properties:

$$\gamma_{\lambda} = \mathrm{C}_{\gamma}\left(\frac{\nu\varepsilon}{\kappa^2}\right)^{1/4} \tag{2}$$

$$V^* = \gamma_{\lambda} \cdot V \tag{3}$$

The constant C_{γ} is equal to 2.1377 [22].

Based on the mass transfer between the fine structures and their surroundings, the mean reaction term becomes:

$$R_i = \frac{\rho\gamma_{\lambda}^2}{\tau^*(1-\gamma_{\lambda}^3)}\,(\omega_i^* - \omega_i^0) \tag{4}$$

where ρ is the density and ω_i is the mass fraction of each species. The EDC model can incorporate detailed chemical mechanisms into turbulent reacting flows and can be used when the assumption of fast chemistry is invalid. However, typical mechanisms are invariably stiff and their numerical integration is computationally costly.

3.2.2. Steady laminar flamelet model

The basic assumption is that instantaneous thermo-chemical state of the fluid is related to a conserved scalar quantity known as the mixture fraction. In this way the species transport equations can be reduced to a transport equation for the mixture fraction ξ and one for its variance ξ'^2:

$$\frac{\partial}{\partial t}(\rho\xi) + \frac{\partial}{\partial x_i}(\rho U_i\xi) = \frac{\partial}{\partial x_i}\left(\frac{\mu_t}{Sc_t}\frac{\partial\xi}{\partial x_i}\right) \tag{5}$$

$$\frac{\partial}{\partial t}(\rho\xi'^2) + \frac{\partial}{\partial x_i}(\rho U_i\xi'^2) = \frac{\partial}{\partial x_i}\left(\frac{\mu_t}{Sc_t}\frac{\partial\xi'^2}{\partial x_i}\right) + 2\frac{\mu_t}{Sc_t}\left(\frac{\partial\xi'^2}{\partial x_i}\right)^2 - C_{\emptyset}\rho\frac{\varepsilon}{\kappa}\xi'^2 \tag{6}$$

The constant $C_{\emptyset}$ inside the dissipation term can be derived by turbulent spectral analysis and is usually set at 2. If the system is not adiabatic, the enthalpy balance equation must be solved:

$$\frac{\partial}{\partial t}(\rho H) + \frac{\partial}{\partial x_i}(\rho U_i H) = \frac{\partial}{\partial x_i}\left(\frac{k_t}{C_P}\frac{\partial H}{\partial x_i}\right) + S_H \quad (7)$$

where k_t and C_p are the thermal conductivity and specific heat of the mixture, and S_H is a generic source term which accounts for the non-adiabatic behavior of the system.

The temperature and thermo-chemical variables are extracted from a flamelet library, in which the temperature and composition corresponding to each value of the mean mixture fraction, mixture fraction variance and enthalpy are stored. The average value of the generic scalar ψ stored in the library is evaluated by the following integral:

$$\psi = \int_0^1 f_\xi(\xi).\psi(\xi, H)d\xi \quad (8)$$

where $f_\xi(\xi)$ is the mixture fraction PDF (probability distribution function) and $\psi(\xi, H)$ represents the relationship between mixture fraction and enthalpy to the scalar ψ. In this work a β-PDF is employed. The function $\psi(\xi, H)$, which takes into account the treatment of complex chemistry, can be modeled following a different approach. In the case of the steady laminar flamelet model the turbulent flame is considered as an ensemble of discrete, steady laminar flames, called flamelets.

3.2.3. Composition PDF transport model

The composition PDF transport model allows simulating finite-rate chemical kinetic effects in turbulent reacting flows as well as flame extinction and ignition. These PDF transport simulations are computationally expensive, but the computational power currently available allows the use of such an approach for two-dimensional simulations.

An alternative to Reynolds-averaging the species and energy equations (which leads to unknown terms for the turbulent scalar flux and the mean reaction rate that needs to be modeled) is to derive a transport equation for their single-point, joint probability density function (PDF) [28]. The main strength of the PDF transport approach is that the highly-nonlinear reaction term is completely closed and does not require modeling. This PDF, denoted by *P*, can be considered to be proportional to the fraction of the time that the fluid spends at each species and temperature state: *P* has N+1 dimensions for the N species and temperature. From the PDF, any thermochemical moment (*e.g.* mean reaction rate or mean or RMS

temperature) can be calculated. The composition PDF transport equation is derived from the Navier-Stokes equations as [29]:

$$\frac{\partial}{\partial t}(\rho P) + \frac{\partial}{\partial x_i}(\rho u_i P) + \frac{\partial}{\partial \psi_k}(\rho S_k P) = -\frac{\partial}{\partial x_i}[\rho \langle u_i'' | \psi \rangle P] + \frac{\partial}{\partial \psi_k}\left[\rho \left\langle \frac{1}{\rho}\frac{\partial J_{i,k}}{\partial x_i} \middle| \psi \right\rangle P\right] \quad (9)$$

where P is the Favre joint PDF of composition, ρ is the mean density of the fluid, u_i is the Favre mean fluid velocity vector, S_k is the reaction rate for species k, ψ is the composition space vector, u_i'' is the fluid velocity fluctuation vector, and $J_{i,k}$is the molecular diffusion flux vector. The generic notation <A|B> indicates the conditional probability of event A, given the occurrence of event B. In Equation (1), the terms on the left-hand side are closed, whereas those on the right-hand side are not and require modeling. The turbulent scalar flux term is modeled by the gradient diffusion assumption:

$$-\frac{\partial}{\partial x_i}[\rho \langle u_i'' | \psi \rangle P] = \frac{\partial}{\partial x_i}\left(\frac{\mu_t}{\rho Sc_t}\frac{\partial P}{\partial x_i}\right) \quad (10)$$

where μ_t is the turbulent viscosity and Sc_t is the turbulent Schmidt number.

In PDF methods, the effect of molecular diffusion on the composition is represented by a mixing model. Two mixing models, the modified curl (MC) model [30,31] and Euclidean minimum spanning tree (EMST) model [32] were used in this study to model mixing at the smallest molecular scales. For the MC model, a few particle pairs are selected at random from all the particles in a cell, and their individual compositions are moved toward their mean composition. The number of particle pairs selected is calculated from the algorithm according to the total number of particles and the local turbulent time scale (k/ε). For each particle pair, a uniform random number β is selected and each particle's composition ∅ is moved toward the pair's mean composition by a factor proportional to β:

$$\emptyset_i^1 = (1-\theta)\emptyset_i^0 + \theta\frac{(\emptyset_i^0 m_i + \emptyset_j^0 m_j)}{(m_i + m_j)} \quad (11)$$

$$\emptyset_j^1 = (1-\theta)\emptyset_j^0 + \theta\frac{(\emptyset_i^0 m_i + \emptyset_j^0 m_j)}{(m_i + m_j)} \quad (12)$$

where $\emptyset_i$ and $\emptyset_j$ are the composition vectors of particles i and j, and m_i and m_j are the masses of particles i and j.

Physically, mixing occurs between fluid particles that are adjacent to each other. The MC mixing model takes no account of this localness, which can be a source of error. The advantage of the Euclidean minimum spanning tree (EMST) model is that it mixes particle pairs that are close to each other in composition space. In this way the model takes into account the physical constraint that mixing occurs between fluid particles that are adjacent to each other. Since scalar fields are locally smooth, particles that are close in composition space are likely to be close in physical space. The particle pairing is determined by a Euclidean minimum spanning tree, which is the minimum length of the set of edges connecting one particle to at least one other particle. The EMST mixing model is more accurate than the MC and interaction by exchange with the mean (IEM) mixing models, but is slightly more computationally expensive. Details on the EMST model can be found in ref. [32].

3.3. Kinetic mechanisms

Due to the recommendations of previous studies [9,10,14], here we adopt only detailed kinetic mechanisms. Two detailed schemes, the GRI-Mech 3.0 [http://www.me.berkeley.edu/gri_mech/] and POLIMI ethylene mechanism [http://creckmodeling.chem.polimi.it/] were evaluated. The GRI-Mech 3.0 mechanism was employed without the NO_x reactions, resulting in 219 reversible reactions relating 36 chemical species. The POLIMI ethylene mechanism used in this work is a reduced version of the combustion mechanism developed at Politecnico di Milano. The complete scheme is available on the aforementioned website. The kinetic model used in this study was described and validated before using a large set of experimental data [33-38], including MILD combustion conditions [10,39]. We recently further validated the kinetic mechanism for ethylene using the coflow flame measurements of McEnally and Pfefferle [40], as discussed by Cuoci *et al.* [41]. The numerical results were found to be in satisfactory agreement with the experimental data, demonstrating the reliability of the kinetic mechanism. Due to the large dimensions of this scheme, it is not suitable for CFD simulations of turbulent flames. Therefore, a reduced version was obtained using an algorithm [42] which combines the reaction path analysis and the directed relation graph method [43]. The reduced model contains 24 species involved in 155 reactions and is able to reproduce the performance of the original mechanism over a wide range of operating conditions ($0.5<\Phi<2.0$) at high temperatures (above 1000 K) and atmospheric pressure.

4. Comparison with experimental measurements

4.1. Effect of turbulence model

Turbulent mixing has a significant effect on the flow field, temperature and turbulence–chemistry interaction. In this study, turbulence was modeled via the RANS approach, using the modified standard *k*-ε (modified SKE), RNG *k*-ε and the Reynolds Stress Model (RSM). Using the modified EDC combustion model [15], discrete ordinates (DO) radiation model and GRI-Mech 3.0 mechanism, calculations for the 3% and 9% O_2 flames were performed. For comparing the different turbulence models in this section, only the GRI-Mech 3.0 mechanism was used. Figure 4 shows radial distributions of the temperature obtained using the three turbulence models at an axial location of 35mm above the jet exit plane for the 3% O_2 flames. It can be observed that discrepancies between the experiments and model predictions are larger for the RNG *k*-ε model. It is noteworthy that the RNG model fails to predict a reaction for all but the pure ethylene flame. The poor agreement of the RNG model was also observed by Christo and Dally [9], Frassoldati *et al.* [10] and De *et al.* [15] for methane and methane/hydrogen jet flames. Moreover, the predictions of the modified SKE and RSM models are almost similar. This figure shows generally good agreement, and excellent agreement between predicted profiles by the modified SKE and RSM with experiments for the C_2H_4/H_2 and C_2H_4/N_2 flames.

The temperature predictions at the axial location of 125mm are more sensitive to the turbulence model used. Nonetheless, the general agreement between the models and the experiments for the 3% O_2 flames is good (refer to Figure S2 (supplementary data)). At this location it is noted that the measured high temperature peak in the C_2H_4/air flame is not captured in the models, which could be a consequence of the complex three-stream mixing (due to the entrainment of surrounding room air). Importantly, the higher centerline temperature for the air-diluted flame is in agreement between the experiments and models. For the 9% O_2 flames, the RSM and modified SKE predict the location of maximum temperature better than RNG *k*-ε model (refer to Figure S3 (supplementary data)). In addition, the RSM model predictions have smaller deviations from the experiments in comparison to the modified SKE predictions. In most cases, however, the measured peak temperature is significantly lower than that from the models. This effect is believed to be an artifact of the lifted characteristics of the experimental flames that has not been captured by the models. The comparison between predicted and measured [16] OH number densities allows better assessment of the effect of the different turbulence models. These results (not shown) demonstrated that the modified SKE and RSM models are more accurate than the RNG *k*-ε model in all these flames. In this study, the modified SKE model is then used in all of the simulations in order to avoid

the additional computational expense of the Reynolds stress model, and to concentrate on the study of turbulence–chemistry interactions.

4.2. Effect of turbulent combustion models

In this section the effect of the models adopted to describe the interactions between turbulence and chemistry is discussed. Experimental measurements [16] are compared to predictions obtained using the models described in section 3.2. Five turbulent combustion models are used to simulate the ethylene flames in the JHC burner using the GRI-Mech 3.0 kinetic mechanism.

4.2.1. Ethylene Flames

Figure 5 illustrates the predictions of the different turbulent combustion models for the 3% O_2 and 9% O_2 ethylene flames, with measured values of temperature and OH number density radial profiles at an axial location of 35 mm and 125mm. It shows that all the models but EDC give good temperature predictions for the 3% O_2 flame at the 35mm location (Fig. 5a). Figure 5b shows a reasonable agreement between predicted and measured OH number density radial profile when the EDC model is used and some discrepancies between the other models and experimental values. The higher OH values of EDC model are expected because of the higher predicted value of temperature at the 35mm location. It should be recognized that there is some uncertainty in the absolute values of the measured OH number density, but importantly the location and features of the OH profiles are consistent between the experiments and the models. Figure 5b also shows that the PDF transport models (modified curl and EMST) predict noticeable equilibrium OH concentration in the coflow region, while the other models predict almost zero value for OH in the coflow stream. At the 125mm axial location, as observed in Fig. 5c, the models of modified EDC, flamelets, PDF transport modified curl and EMST predict the temperature profile reasonably well, but the EDC model noticeably over-predicts the temperature peak. In addition, noticeable discrepancies with measured values of OH number density can be observed for all the used models as shown in Fig. 5d. This could be a result of the complex three-stream mixing with the surrounding air that is difficult to incorporate into the models, as already noted by Christo and Dally [9]. For the 9% O_2 flames, all models tend to overestimate the magnitude of temperature peak. This discrepancy is likely a result of the lifted flame behavior that was observed in the experiments which has not been replicated in the models. Interestingly, all models generally provide good agreement with experiment. Figure 5f reveals that the EDC model can predict accurately the magnitude of OH number density while the flamelets and PDF transport models give better predictions of the peak location of OH concentration.

4.2.2. Ethylene/hydrogen Flames

A comparison between the modeling and experimental data is presented in Fig. 6 for the two ethylene-hydrogen flames (3% O_2 and 9% O_2 in the coflow) and two axial locations. The figure shows that for the 3% O_2 flame, the predicted temperature of the modified EDC, PDF transport modified curl and EMST models at 35mm and 125mm are in good agreement with experimental measurements. Deviations in the absolute values of OH profiles from the experiments are quite large for the all models used, though the locations of the peaks are in agreement. For the 9% O_2 flame, the results of all models except EDC show reasonable agreement in comparison to experimental temperature measurements. In addition, the OH number density values in the 9% O_2 flame have comparable magnitude with experimental measurements for all of the models. Again, similar to the observation for the pure ethylene flames, the conserved scalar based models give a better prediction of the peak location of OH concentration.

4.2.3. Ethylene/air Flames

Figure 7 shows the temperature and OH number density profiles of 3% and 9% O_2 flames at 35mm and 125mm for the ethylene-air fuel case. As can be seen from Fig. 7a, the modified EDC and PDF transport EMST give satisfactory predictions of temperature at 35mm for the 3% O_2 flame. In addition, the EDC model provides good prediction of magnitude of temperature peak, but the shape (width) of temperature profile is not fully consistent with experimental trend. In this partially premixed case, it can be also observed that the flamelets model is too reactive in the region close to the axis and the prediction of this model is not accurate at location of 35 mm. Figure 7b reveals that the EDC and modified EDC models provide reasonable OH values in 3% O_2 flame at 35mm. Also in this case, the OH magnitude in the coflow stream for PDF transport models is comparable to experimental values, while the other models predict much lower OH values in the coflow stream. Figure 7c shows that the predicted temperature profiles are in reasonable agreement for all combustion models, but the shape of the profiles are not correctly predicted when compared with the experiments. All combustion models underestimate the OH number density at 125mm. It is important to note that Medwell *et al.* [16] showed that the influence of the coflow persists ~100 mm downstream of the jet exit plane and that beyond this point the surrounding air begins to mix with the jet and coflow. For this reason, these discrepancies may be related to the effect of the turbulence model and especially the boundary conditions adopted for the coflow and surrounding air inlets (see Fig. 2). This discussion, already presented in detail by Frassoldati *et al.* [10] and Aminian *et al.* [14], is outside the scope of this work, which focuses mainly on the effect of turbulent combustion models

on the CFD predictions. For the 9% O_2 flame, it can be seen that the EDC, modified EDC and flamelet models are too reactive and over-predict the temperature and OH number density at 35mm. Against these models, the PDF transport approach yield an accurate prediction of temperature and OH profiles for the 9% O_2 flame, particularly the EMST model. It can be observed that the (apparent) liftoff height is very sensitive to the model adopted.

4.2.4. Ethylene/nitrogen Flames

Figure 8 illustrates the temperature and OH number density profiles of 3% and 9% O_2 flames at 35mm and 125mm for ethylene-nitrogen fuel. As expected, due to the inert addition there is a lower reactivity in the ethylene-nitrogen flame with respect to other fuels. The apparent liftoff height (not presented in this paper) seems correctly predicted by all models. For the 3% O_2 flame, all combustion models give an accurate temperature prediction at 35mm, but the prediction of OH is not satisfactory and there is a large discrepancy between OH modeling results and measurements. The modeling results indicate that the flame is lifted and that there are no reactions at the location. Experimentally, however, despite the visual appearance of a lifted flame, a reaction zone was indeed recorded in this region. For the 3% O_2 flame at 125mm, the models generate a reasonable prediction of temperature and OH number density. The 9% O_2 in the coflow stream makes this flame more reactive than the equivalent 3% case. Nonetheless, these flames still visually appeared lifted during the experiments. This effect is largely overestimated by EDC, modified EDC and flamelets models, while it is correctly predicted by the PDF transport models.

Overall, the results demonstrate that the modified EDC and PDF transport (EMST and MC) models are adequate for temperature prediction in the 3% O_2 flames of all four fuels studied. For the 3% O_2 flames, all models under-predict the magnitude of the OH peak, but the PDF transport models give a better prediction of location of OH concentration peak. In addition, the values of OH number density in the coflow stream predicted by PDF transport models are more satisfactory than the other models for 3% flames. For the 9% O_2 flame of different fuels, the PDF transport models yield reasonably good agreement with experiments for the temperature and OH number density.

4.2.5. Effect of fuel composition

Figure 9 shows a comparison between the measured peak values of temperature and OH concentration and the corresponding predictions of the models for the different flames. In this way, this figure summarizes the results already presented in more detail in the previous figures, but allows the trends

associated with the changes in fuel composition to be highlighted. It is interesting to observe that at a distance of 35 mm from the inlet, the maximum temperature is a good indicator of the reactivity of the system. The experimental values reported in Fig. 9a clearly show that flame number 3 (partially premixed C_2H_4/air) is the most reactive. All the models are able to reproduce this trend. The PDF transport models significantly underestimate the temperature peak for flame 3, whilst giving satisfactory predictions for the other flames. It is also possible to observe that the EDC model overestimates the reactivity for flame 1 (C_2H_4) and flame 2 (C_2H_4/H_2), while it is in better agreement with measured values for the diluted C_2H_4/N_2 flame. As already observed, the modified EDC provides better predictions in these conditions. This is not surprising since this modification of the EDC model was proposed by De *et al.* [15] for methane under MILD combustion conditions. In this work we extended the validation of the model to ethylene mixtures. The flamelets model does not satisfactorily predict the trend of the temperature peak with the fuel composition, especially for the ethylene/air and ethylene/hydrogen flames. As already discussed, the OH concentration is under-estimated by the models, which are not able to explain the large OH peak of the ethylene/hydrogen flame at 35 mm. The results at 125 mm could be affected by the entrainment of the surrounding air into the flame, which is difficult to accurately capture in the models. Some of the deviations presented in Fig. 9 can be, at least partially, explained on this basis. Figure 9 also shows the comparison of temperature peaks and OH concentrations for the 9% O_2 flames (Fig. 9 e and f). It is evident that only the PDF transport models (MC and EMST) are able to characterize the reactivity of the system in these conditions. The ethylene/hydrogen flame shows the highest temperature peak, while the ethylene/air flame shows a relatively low temperature peak compared with the 3% O_2 case. The EDC and the flamelet model do not correctly describe the system's reactivity and predict a shorter liftoff height, therefore over-estimating the temperature peak. The same analysis applies to the OH peaks.

To better analyze the effect of the turbulent combustion model on the OH predictions, Fig. 10 shows the OH distribution in the flame region close to the burner exit plane. This comparison confirms that the EDC model predicts an attached flame for all the conditions, while the PDF model shows a significant liftoff height for the ethylene flames diluted with air or nitrogen. This different behavior is clearly evident in the OH predictions discussed in Fig. 9. It is interesting to note that experimentally the apparent liftoff for the 9% O_2 flames is 26 mm for the C_2H_4 flame and 33 and 34 mm for the C_2H_4/Air and C_2H_4/N_2 flames, respectively. This behavior is quite well reproduced by the PDF model. On the contrary, the C_2H_4/H_2 flame is attached and this is not completely captured by the model. The 3% O_2 flames are all weakly reactive but all attached to the burner, as experimentally observed. Both the EDC and PDF models correctly predict this behavior, based on the analysis of the OH plots. Medwell *et al.* [16] showed that

rather than referring to them as lifted, these ethylene flames can be better described as having a transition in the reaction. The apparent liftoff height corresponds to a transition of weak to strong OH levels. As such, rather than identifying a "liftoff" height, it is more appropriate to refer to this as a transition point. The general observations relating to this transition point seem to be analogous to conventional lifted flame zones.

Table 2 reports the estimated error of the predicted apparent liftoff heights (transition points), for the different turbulent combustion models. This deviation is simply calculated as the difference (in axial space) between the 35 mm location and the region where the radial predicted temperature profile matches the one measured at 35 mm. As an example, for the ethylene flame, the EDC model largely over-predicts the temperature profile at 35 mm, especially for the 9% O_2 flame (see Fig. 5a and 5e). For this reason, to match the measured and predicted temperature profiles, it is necessary to shift the axial position towards the inlet by 25 mm (*i.e.* using the profile at the 10 mm axial location) for the 3% case and of 30.8 mm for the 9% case. The shift is larger for the 9% case because the temperature is largely over-estimated by the model. We use this shift as an indicator of the error in the transition points of the flames. It is important to notice that this indicator shows a deviation which can be due both to an error in the predicted liftoff height and in the reactivity of the flame. Since they are all attached, the negative values of ELOE for the 3% O_2 flames are likely to indicate that the EDC model in particular over-estimates the reactivity of the flame and the position of the transition point between weak and strong reactivity. Also in these cases, the PDF models are in better agreement with the experiments.

The comparison shows the better agreement of the PDF transport models compared with EDC and flamelet models, which is likely due to their ability to characterize localized extinction or intermittency phenomena. Another observation is that the modified EDC, compared to the original model, improves the predictions which become very similar to the ones of the flamelet model. Finally, the errors are larger for the 9% O_2 cases relative to 3% O_2.

4.3. Formation and consumption of CH_2O

Formaldehyde is an important intermediate in the oxidation of hydrocarbons. It is also formed in significant amounts in the low temperature combustion of hydrocarbons and oxygenated biofuels. It is interesting to note that the premixing of O_2 with the fuel allows CH_2O to be formed in regions of the flame where the local conditions make its consumption a slow process. The expected effect of premixing

is to increase the peak of formaldehyde in the flame, up to five times as compared to purely diffusive flames [44]. A detailed analysis of CH_2O formation in flames in a heated and diluted oxidant stream has been presented by Medwell *et al.* [45] using laminar flame calculations. They showed that under MILD conditions O_2 penetrates the reaction zone, leading to partial premixing and thus contributing to the improved flame stability under these conditions.

Formaldehyde profiles were measured by Medwell *et al.* [16] and provided in arbitrary units for the JHC burner. Since the experimental measurements are not quantitative, we decided to apply a scaling factor to the predicted CH_2O number density. For each condition (figure), the scaling factor is calculated to match the measured and predicted CH_2O peak in the pure ethylene flame. The same factor is then applied to the predicted profiles of the other flames. In this way, it is possible to compare the shape of the profiles and the effect of the fuel on the formation of formaldehyde. Figure 11 shows that the modified EDC and the PDF models are able to correctly characterize the relative formation of CH_2O in the pure ethylene and in the partially premixed flames. The relatively large amount of formaldehyde on the axis of the flame is not predicted by the models. Figure 11f summarizes the results in terms of peak CH_2O. Due to the normalization, all the predicted CH_2O peaks coincide with the measured peak CH_2O value for the C_2H_4 flame. It is quite evident that all models succeeded in predicting the effect of fuel composition on the formation of CH_2O. It is interesting to observe that the effect of H_2 is to reduce the formation of CH_2O. This is expected as the availability of C atoms is reduced due to the dilution with hydrogen. The same effect can be observed for N_2 dilution. On the contrary, the partial premixing with air (O_2) has a relevant chemical effect which is properly captured by the models. To compare the effect of the kinetic mechanism, Fig. 12 shows the predicted CH_2O formed in two counterflow laminar flames calculated in conditions representative of those of the experiments. The oxidant has the temperature and composition of the coflow used in the JHC flames and the fuel is pure ethylene or ethylene/air. It is evident that the formation of CH_2O in the partially premixed case is significantly larger and that it occurs earlier (closer to the fuel inlet), while in the diffusive flame CH_2O is mainly formed in the lean side of the flame front. The CH_2O predicted by the GRI-Mech 3.0 model is larger than the amount predicted by the POLIMI model in the partially premixed flame. The reaction flux analyses presented in Figs 13 and 14 clearly show the difference between ethylene premixed and diffusion flames. Both for POLIMI and GRI-Mech 3.0, the consumption of ethylene proceeds through the formation of vinyl radicals which subsequently form acetylene. The fate of vinyl radicals is different when O_2 is available in the system at the early stage of ethylene consumption. Vinyl radicals react with O_2 to produce CH_2CHO, which subsequently forms CH_2CO. Ketene then forms formaldehyde either directly (POLIMI) or via CH_3 formation and oxidation.

The comparison of Figs 13 and 14 also explains the differences between partially premixed and diffusive flames. It is even more pronounced at the 125mm axial location (compared with the 35 mm location) that the partially premixed flame is characterized by the largest amount of CH_2O (refer to Figure S4 (supplementary data) for further details). The effect of fuel composition is quite well captured by the combustion models. Only the flamelet model failed in predicting this observed value for the partially premixed flame. For the 9% O_2 flame the previous findings are confirmed at 35mm: the PDF transport and modified EDC models provide a satisfactory agreement with the experimental data while the flamelets model shows a large deviation especially in the partially premixed conditions (refer to Figure S5 (supplementary data) for further details). Also in this case the modified EDC improves the agreement with the measurements. In fact, the EDC overestimates the increase of CH_2O when air is premixed with the fuel. This deviation was not present in the 3% O_2 flame.

4.4. Effect of the kinetic mechanism

The effect of the kinetic mechanism on the modeling was investigated by comparing predictions using two different mechanisms, POLIMI and GRI-Mech 3.0. First we discuss the difference between the two mechanisms in laminar flame conditions, then in the ethylene turbulent flames studied in this work.

Figure 15a shows a comparison between experimental measurements [46-50] and model predications of laminar flame speed of ethylene in air for the kinetic mechanisms considered in this study. The flame speeds were calculated using the OpenSMOKE code [51]. A more detailed description on the flame speed calculations can be found in ref. [52], which also contains an extensive validation of the POLIMI model. Two observations can be made: first, it is quite evident the larger reactivity of ethylene compared to methane, whose maximum flame speed in these conditions is 35-38 cm/s under these conditions. Second, it can be observed that the reduced C_2H_4 model developed at Politecnico di Milano is able to correctly predict the reactivity of ethylene and the velocity of flame propagation. On the other hand, GRI-Mech 3.0 – a mechanism which was originally developed for methane and natural gas combustion – significantly over-estimates the flame speed. The same difference in the reactivity of the flame can be observed in Fig. 15b, where the flame speed is calculated for a mixture of ethylene and hot and diluted air. The oxidizer contains 9% O_2 and has the same composition of the oxidizer used in the coflow of the JHC burner experiments discussed in this paper. Referring back to the earlier discussion surrounding liftoff height, it may be deduced that the liftoff behavior was not captured in the model also as a result of the excessively high flame speed when using the GRI-Mech 3.0 mechanism.

The EDC combustion model and modified SKE turbulence model have been adopted in simulations of the 9% O_2 ethylene flames and show that the temperature and OH number density profiles are very similar for these two mechanisms (refer to Figure S6 (supplementary data) for further details). It is interesting to note that, despite differences in the laminar flame speed for the two chemistry models considered, the choice of kinetics does not significantly influence the reaction zone profiles in the turbulent flame conditions. This suggests that the turbulence–chemistry interactions play a major role that largely supersedes the differences in the kinetic schemes. On the contrary, Fig. 16 shows that the tendency of GRI-Mech 3.0 to form a larger amount of CH_2O is also evident in the turbulent partially premixed flame. For the 3% O_2 coflow cases, it is difficult to stabilize the flame with the POLIMI mechanism and the EDC turbulent combustion model. This effect, which prevents a wide range of comparisons using the POLIMI kinetic scheme, may be due to the already discussed lower reactivity of the POLIMI mechanism with respect to the GRI-Mech 3.0, and to the difficulty of EDC in describing the mechanism of jet flame stabilization, as already noted by [53].

It is important to note that although PDF transport models provide simulation results which are in better agreement with experimental measurements the EDC remains a valuable model. The interest in EDC is mainly motivated by the advantages related to its relatively low computational requirements. This is important, especially when referring to CFD modeling of real three-dimensional combustors. The complexity and the size of the computational grid associated with such a geometry makes it difficult to use PDF transport models with detailed chemistry.

5. Conclusions

Turbulent nonpremixed jet flames issuing into a heated and highly diluted coflow were investigated in this study using a CFD code (FLUENT 12.1.4). An extensive set of simulation results is presented for several ethylene flames, either undiluted or diluted with hydrogen, air or nitrogen, to highlight the effect of using different turbulent combustion models and kinetic schemes (GRI-Mech 3.0 and POLIMI). The predictions of the flame structure using the two kinetic mechanisms are very similar. In the case of the 3% O_2 flames, using the POLIMI mechanism with the EDC model led to flame extinction. This behavior is attributed to the difficulties of the EDC model in predicting the jet flame stabilization [53]. The modified k-ε model succeeded in simulating the fuel jet fluid dynamics flame structure. Thermal radiation was included in the model using the discrete ordinate model. The comparison between the predicted and the

measured mean temperature profiles showed a systematic deviation for the standard EDC model. This model is found to over-estimate the reactivity of the flame, both in the 3% and 9% O_2 cases. In other words, the EDC tends to under-predict liftoff height. The predictions are significantly improved by using a modified version of the EDC [15,24], which was developed for MILD combustion conditions. The modeling results demonstrate that the modified EDC yields reasonable results with a relatively low computational effort. The agreement between measurements and predictions of the PDF transport and modified EDC models is generally better than for the flamelet model. A comparative study is also presented for the impact of two micro-mixing models in transported scalar PDF simulations of these flames. The micro-mixing models are MC (modified curl) and EMST (Euclidean minimum spanning tree). In general the difference between the predictions of the two PDF models is not significant. The predictions are in good agreement with the measurements, and are improved especially for the apparent liftoff heights and the temperature peaks. The effect of the fuel composition on the CH_2O formation is also discussed and shows good agreement.

Acknowledgements

The research activity at Politecnico di Milano was supported by “Progetto 5 per mille” code D41J10000490001. The authors thank A/Prof. Bassam Dally for his assistance with the experimental component of this project. The financial support of the University of Adelaide and the Australian Research Council is gratefully acknowledged.

References

[1] A. Cavaliere, M. de Joannon, Mild combustion, Prog. Energy Combust. Sci. 30 (2004) 329-366.

[2] T. Hasegawa, S. Mochida, A.K. Gupta, Development of advanced industrial furnace using highly preheated air combustion, J. Propul. Power 18 (2002) 233-239.

[3] J.A. Wünning, J.G. Wünning, Flameless oxidation to reduce thermal NO formation, Prog. Energy Combust. Sci. 23 (1997) 81-94.

[4] R. Weber, A.L. Verlaan, S. Orsino, N. Lallemant, On emerging furnace design methodology that provides substantial energy savings and drastic reduction in CO_2, CO and NO_x emissions, J. Inst. Energy 72 (1999) 77-83.

[5] M. Katsuki, T. Hasegawa, Science and technology of combustion in highly preheated air, Proc. Combust. Inst. 27 (1998) 3135-3146.

[6] C. Galletti, A. Parente, M. Derudi, R. Rota, L. Tognotti, Numerical and experimental analysis of NO emissions from a lab-scale burner fed with hydrogen-enriched fuels and operating in MILD combustion, Int. J. Hydrogen Energy 34 (2009) 8339–8351.

[7] E. Oldenhof, M.J. Tummers, E.H. van Veen, D.J.E.M. Roekaerts, Ignition kernel formation and lift-off behaviour of jet-in-hot-coflow flames, Combust. Flame 157 (2010) 1167-1178.

[8] A. Rebola, M. Costa, P.J. Coelho, Experimental evaluation of the performance of a flameless combustor, Appl. Thermal Eng. 50 (2013) 805–815.

[9] F.C. Christo, B.B. Dally, Modeling turbulent reacting jets issuing into a hot and diluted coflow, Combust. Flame 142 (2005) 117-129.

[10] A. Frassoldati, P. Sharma, A. Cuoci, T. Faravelli, E. Ranzi, Kinetic and fluid dynamics modeling of methane/hydrogen jet flames in diluted coflow, Appl. Thermal Eng. 30 (2010) 376-383.

[11] S.H. Kim, K.Y. Huh, B.B. Dally, Conditional moment closure modeling of turbulent nonpremixed combustion in diluted hot coflow, Proc. Combust. Inst. 30 (2005) 751-757.

[12] B. Danon, E.-S. Cho, W. de Jong, D.J.E.M. Roekaerts, Parametric optimization study of a multi-burner flameless combustion furnace, Appl. Thermal Eng. 31 (2011) 3000-3008.

[13] B. Danon, E.-S. Cho, W. de Jong, D.J.E.M. Roekaerts, Numerical investigation of burner positioning effects in a multi-burner flameless combustion furnace, Appl. Thermal Eng. 31 (2011) 3885–3896.

[14] J. Aminian, C. Galletti, S. Shahhosseini, L. Tognotti, Key modeling issues in prediction of minor species in diluted-preheated combustion conditions, Appl. Thermal Eng. 31 (2011) 3287-3300.

[15] A. De, E. Oldenhof, P. Sathiah, D.J.E.M. Roekaerts, Numerical simulation of Delft-jet-in-hot-coflow (DJHC) flames using the Eddy dissipation concept model for turbulence–chemistry interaction, Flow Turbulence Combust. doi: 10.1007/s10494-011-9337-0.

[16] P.R. Medwell, P.A.M. Kalt, B.B. Dally, Imaging of diluted turbulent ethylene flames stabilized on a Jet in Hot Coflow (JHC) burner, Combust. Flame 152 (2008) 100–113.

[17] P.R. Medwell, P.A.M. Kalt, B.B. Dally, Simultaneous imaging of OH, formaldehyde, and temperature of turbulent nonpremixed jet flames in a heated and diluted Coflow, Combust. Flame 148 (2007) 48–61.

[18] B.B. Dally, D.F. Fletcher, A.R. Masri, Flow and mixing fields of turbulent bluff-body jets and flames, Combust. Theory Model. 2 (1998) 193-219.

[19] D.C. Wilcox, Turbulence Modeling for CFD, 3rd ed., DCW Industries Inc., 2006, ISBN 978-1-928729-08-2.

[20] I.R. Gran, I.S. Ertesvag, B.F. Magnussen, Influence of turbulence modeling on predictions of turbulent combustion, AIAA J. 35 (1997) 106 –110.

[21] E.H. Chui, G.D. Raithby, Computation of radiant heat transfer on a nonorthogonal mesh using the finite-volume method, Numer. Heat Transfer B 23(1993) 269-288.

[22] B.F. Magnussen, On the structure of turbulence and a generalized eddy dissipation concept for chemical reactions in turbulent flow, 19th AIAA Aerospace Science Meeting, St. Louis, Missouri, 1981.

[23] I.S. Ertesvåg, B.F. Magnussen, The Eddy Dissipation Turbulent Energy Cascade Model, Comb. Sci. Tech. 159 (2001) 213-236.

[24] J. Aminian, C. Galletti, S. Shahhosseini, L. Tognotti, Modelling a reacting jet in hot diluted coflow: evaluation of the turbulence/chemistry interaction model, Proc. of the 5th European Combustion Meeting, pp. 1-6, Cardiff, UK, 2011.

[25] N. Peters, Turbulent combustion, first ed., Cambridge University Press, Cambridge, 2000.

[26] T. Poinsot, D. Veynante, Theoretical and numerical combustion, second ed., R.T. Edwards Inc., Philadelphia, 2005.

[27] S.B. Pope, Computationally efficient implementation of combustion chemistry using in situ adaptive tabulation, Combust. Theory Model. 1 (1997) 41-63.

[28] Fluent®, Fluent Inc, Lebanon, NH, USA, 2005.

[29] S.B. Pope, PDF methods for turbulent reactive flows, Prog. Energy Combust. Sci., 11 (1985) 119-192.

[30] J. Janicka, W. Kollmann, A Two-Variable Formulation for the Treatment of Chemical Reactions in Turbulent H_2-Air Diffusion Flames, Proc. Combust. Inst. 17, pp. 421–430, Pittsburgh, PA, 1978.

[31] P. A. Nooren, H. A. Wouters, T. W. J. Peeters, D. Roekaerts, U. Maas, D. Schmidt, Monte carlo pdf modeling of a turbulent natural-gas diffusion flame, Combust. Theory Model. 1 (1997) 79-96.

[32] S. Subramaniam, S. B. Pope, A Mixing Model for Turbulent Reactive Flows Based on Euclidean Minimum Spanning Trees, Combust. Flame, 115 (1998) 487-514.

[33] E. Ranzi, A. Sogaro, P. Gaffuri, G. Pennati, C. K. Westbrook, W. J. Pitz, A new comprehensive reaction mechanism for combustion of hydrocarbon fuels, Combust. Flame 99 (1994) 201-211.

[34] E. Ranzi, M. Dente, G. Bozzano, A. Goldaniga, T. Faravelli, Lumping procedures in detailed kinetic modeling of gasification, pyrolysis, partial oxidation and combustion of hydrocarbon mixtures, Prog. Energy Combust. Sci. 27 (2001) 99-139.

[35] A. Frassoldati, T. Faravelli, E. Ranzi, K. Kohse-Höinghaus, P.R. Westmoreland, Kinetic modeling study of ethanol and dimethyl ether addition to premixed low-pressure propene–oxygen–argon flames, Combust. Flame 158 (2011) 1264–1276.

[36] A. Frassoldati, T. Faravelli, E. Ranzi, Ignition Combustion and Flame Structure of Carbon Monoxide/Hydrogen Mixtures. Note 1: Detailed Kinetic Modeling of Syngas Combustion also in Presence of Nitrogen Compounds, Int. J. Hydrogen Energy, 32 (2007) 3471-3485.

[37] E. Ranzi, A. Frassoldati, S. Granata, T. Faravelli, Wide-Range Kinetic Modeling Study of the Pyrolysis, Partial Oxidation, and Combustion of Heavy n-Alkanes, Ind. Eng. Chem. Res. 44 (2005) 5170-5183.

[38] W. Ren, D.F. Davidson, R.K. Hanson, IR laser absorption diagnostic for C_2H_4 in shock tube kinetics studies, Int. J. Chem. Kinet. 44 (2012) 423-432.

[39] M. de Joannon, A. Cavaliere, T. Faravelli, E. Ranzi, P. Sabia, A. Tregrossi, Analysis of process parameters for steady operations in methane mild combustion technology, Proc. Combust. Inst. 32 (2009) 585–591.

[40] C.S. McEnally, L.D. Pfefferle, Experimental study of nonfuel hydrocarbons and soot in coflowing partially premixed ethylene/air flames, Combust. Flame 121 (2000) 575-592.

[41] A. Cuoci, A. Frassoldati, T. Faravelli, E. Ranzi, Numerical modeling of laminar coflow flames with detailed kinetics, XXXIV Meeting of the Italian Section of the Combustion Institute, Rome, October 2011, doi:10.4405/34proci2011.I19

[42] V. Ceruleo, MSc Dissertation, Politecnico di Milano, Italy (2011).

[43] T.F. Lu, C. K. Law, A directed relation graph method for mechanism reduction, Proc. Combust. Inst. 30 (2005) 1333-1341.

[44] C.S. McEnally, L.D. Pfefferle, Experimental study of nonfuel hydrocarbon concentrations in coflowing partially premixed methane/air flames, Combust. Flame 118 (1999) 619-632.

[45] P. R. Medwell, P. A. M. Kalt, B. B. Dally, Reaction Zone Weakening Effects under Hot and Diluted Oxidant Stream Conditions, Combust. Sci. Tech. 181 (2009) 937–953.

[46] T. Hirasawa, C.J. Sung, A. Joshi, Z. Yang, H. Wang, C.K. Law, Determination of laminar flame speeds using digital particle image velocimetry: Binary Fuel blends of ethylene, n-Butane, and toluene, Proc. Combust. Inst. 29 (2002) 1427–1434.

[47] F.N. Egolfopoulos, D.L. Zhu, C.K. Law, Experimental and numerical determination of laminar flame speeds: Mixtures of C2-hydrocarbons with oxygen and nitrogen, Proc. Combust. Inst. 23 (1991) 471–478.

[48] G. Jomaas, X.L. Zheng, D.L. Zhu, C.K. Law, Experimental determination of counterflow ignition temperatures and laminar flame speeds of C_2–C_3 hydrocarbons at atmospheric and elevated pressures, Proc. Combust. Inst. 30 (2005) 193–200.

[49] M.I. Hassan, K.T. Aung, O.C. Kwon, G.M. Faeth, Properties of Laminar Premixed Hydrocarbon/Air Flames at Various Pressures, J. Propuls. Power 14 (1998) 479–488.

[50] K. Kumar, G. Mittal, C-J. Sung, C. K. Law, An experimental investigation of ethylene/O_2/diluents mixtures: Laminar flame speeds with preheat and ignition delays at high pressures, Combust. Flame 153 (2008) 343–354.

[51] A. Cuoci, A. Frassoldati, T. Faravelli, E. Ranzi, OpenSMOKE: numerical modeling of reacting systems with detailed kinetic mechanisms, XXXIV Meeting of the Italian Section of the Combustion Institute, Rome (Italy) ,October 24-26th (2011). doi:10.4405/34proci2011.II23

[52] E. Ranzi, A. Frassoldati, R. Grana, A. Cuoci, T. Faravelli, A. P. Kelley, C. K. Law, Hierarchical and Comparative Kinetic Modeling of Laminar Flame Speeds of Hydrocarbon and Oxygenated Fuels, Prog. Energy Combust. Sci. 38 (2012) 468-501.

[53] S. Zahirović, R. Scharler, P. Kilpinen, I. Obernberger, Validation of flow simulation and gas combustion sub-models for the CFD-based prediction of NOx formation in biomass grate furnaces, Combust. Theory Model. 15 (2011) 61-87.

Figure Captions:

Fig.1. JHC burner schematic diagram [16,17].

Fig. 2. Two-dimensional view of the computational domain and boundary conditions. Boundary conditions are indicated in the figure. Walls are assumed adiabatic.

Fig. 3. Experimental photographs [16] and predicted temperature field (the modified EDC combustion model, modified SKE turbulence model, GRI-Mech 3.0 kinetic mechanism are used in generating the temperature field) of pure ethylene flames at Re_{jet} = 10,000 for two coflow O_2 levels. Dotted lines show the locations of the measurements, which were taken along the axial height 35 and 125 mm from the inlet.

Fig. 4. Effect of turbulence models (modified EDC [15] and GRI-Mech 3.0 mechanism used for the combustion modeling and Discrete Ordinates (DO) model for radiation): comparison between experimental measurement and model predictions at axial location of 35mm for the 3% O_2 coflow oxidant stream and different fuels: (a) C_2H_4, (b) C_2H_4/Air, (c) C_2H_4/H_2, (d) C_2H_4/N_2

Fig. 5. Effect of turbulent combustion models (adopting the modified SKE turbulence model, GRI-Mech 3.0 mechanism and (DO) radiation model): comparison between experimental measurement [16] and model predictions (temperature (a,c,e) and OH number density (b,d,f)) for 3% O_2 and 9% O_2 ethylene flames.

Fig. 6. Effect of turbulent combustion models (adopting the modified SKE turbulence model, GRI-Mech 3.0 mechanism and (DO) radiation model): comparison between experimental measurement [16] and model predictions (temperature (a,c,e) and OH number density (b,d,f)) for 3% O_2 and 9% O_2 ethylene/hydrogen flames.

Fig. 7. Effect of turbulent combustion models (adopting the modified SKE turbulence model, GRI-Mech 3.0 mechanism and (DO) radiation model): comparison between experimental measurement [16] and model predictions (temperature (a,c,e) and OH number density (b,d,f)) for 3% O_2 and 9% O_2 ethylene/air flames.

Fig. 8. Effect of turbulent combustion models (adopting the modified SKE turbulence model, GRI-Mech 3.0 mechanism and (DO) radiation model): comparison between experimental measurement [16] and model predictions (temperature (a,c,e) and OH number density (b,d,f)) for 3% O_2 and 9% O_2 ethylene/nitrogen flames.

Fig. 9. Maximum temperature and OH number density of experimental measurement [16] and model predictions (different turbulent combustion models) for studied flames. Flame number 1: (C_2H_4), flame number 2: (C_2H_4/H_2), flame number 3: (C_2H_4/air) and flame number 4: (C_2H_4/N_2).

Fig. 10. Predicted OH number densities for the studied flames using the EDC and PDF-EMST models.

Fig. 11. Experimental [16] and modeling mean radial profile of formaldehyde for 3% flame at axial location of 35mm. Orange: C_2H_4, blue: C_2H_4/H_2, black: C_2H_4/air and green: C_2H_4/N_2. Lines: experimental results and dashed lines: modeling results, (panels a-e). Panel f: comparison between

measured and predicted maximum CH_2O (of panels a-e) using different turbulent combustion models. Flame number 1: (C_2H_4), flame number 2: (C_2H_4/H_2), flame number 3: (C_2H_4/air) and flame number 4: (C_2H_4/N_2).

Fig. 12. Comparison between formaldehyde mole fraction of two kinetic mechanisms (GRI-Mech 3.0 and POLIMI) found from laminar flame calculation. 9% O_2 coflow oxidant stream. T_{oxi} = 1100 K. a ≈ 200 s^{-1}.

Fig. 13. a. Reaction Path Analysis for GRI 3.0 and the conditions of Figure 12a (diffusion flame), b. Reaction Path Analysis for GRI-Mech 3.0 and the conditions of Figure 12b (partially premixed flame)

Fig. 14. a. Reaction Path Analysis for POLIMI and the conditions of Figure 12a (diffusion flame), b. Reaction Path Analysis for POLIMI and the conditions of Figure 12b (partially premixed flame)

Fig. 15. a. Laminar flame speed of ethylene in air at 1 atm and 300 K. Comparison between GRI-Mech 3.0 and POLIMI predicted values with experimental data [46-50], b. Laminar flame speed of ethylene in hot diluted air (9% O_2) at 1 atm and initial temperature of 1000 K. Comparison between GRI-Mech 3.0 and POLIMI predicted values.

Fig. 16. Experimental and modeling mean radial profile of formaldehyde for 9% flame at axial location of 35mm. Orange: C_2H_4, blue: C_2H_4/H_2, black: C_2H_4/air and green: C_2H_4/N_2. Lines: experimental results and dashed lines: modeling results obtained using the EDC model and two different kinetic mechanisms. (panels a and b). Predicted and measured maximum CH_2O using two kinetic mechanisms. Flame number 1: (C_2H_4), flame number 2: (C_2H_4/H_2), flame number 3: (C_2H_4/air) and flame number 4: (C_2H_4/N_2) (Panel c).

Table captions:

Table 1. Operating conditions of two inlet streams (on a molar basis) for the different case studies.

Table 2. Estimated apparent Lift Off (transition points) Error (ELOE) (units: mm) of different turbulent combustion models. The estimate is based on the comparison of predicted and measured temperatures.

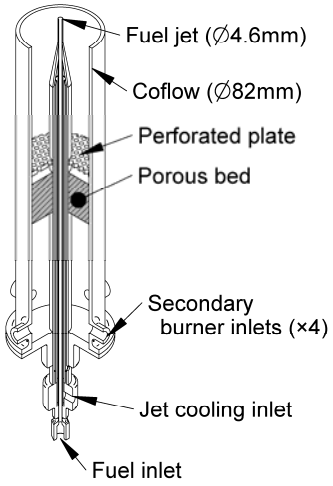

Fig.1. JHC burner schematic diagram [16,17].

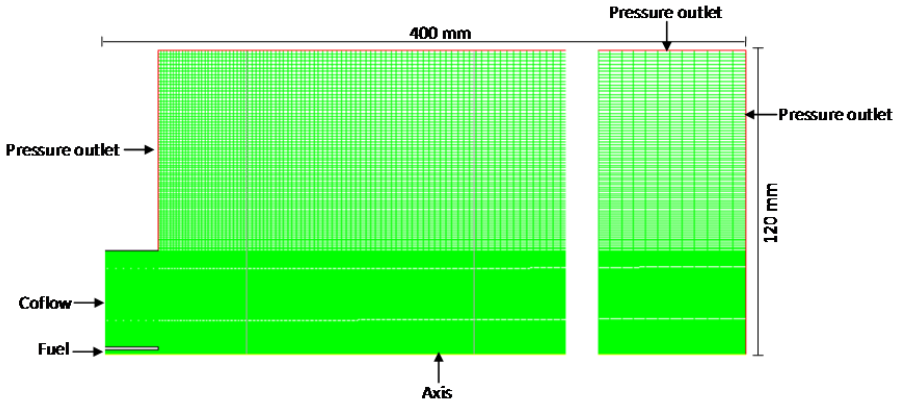

Fig. 2. Two-dimensional view of the computational domain and boundary conditions. Boundary conditions are indicated in the figure. Walls are assumed adiabatic.

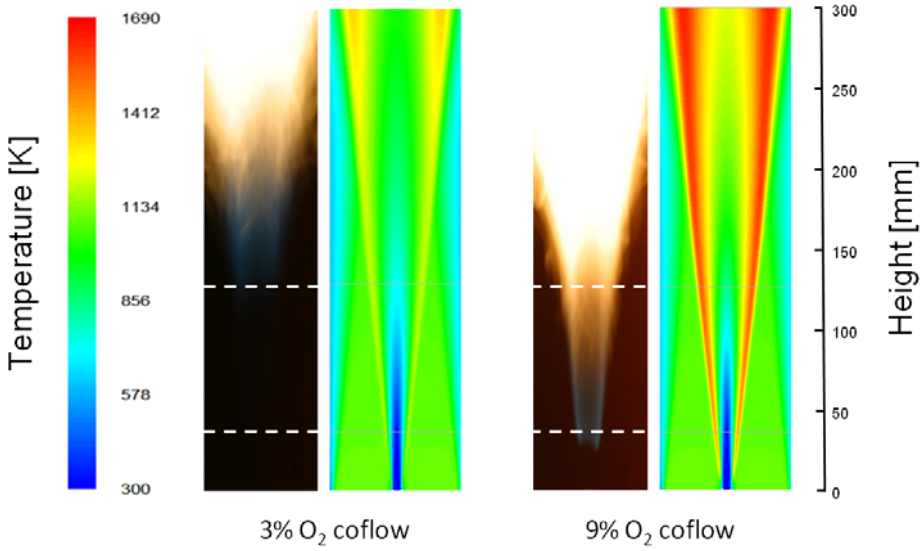

Fig. 3. Experimental photographs [16] and predicted temperature field (the modified EDC combustion model, modified SKE turbulence model, GRI-Mech 3.0 kinetic mechanism are used in generating the temperature field) of pure ethylene flames at Re_{jet} = 10,000 for two coflow O_2 levels. Dotted lines show the locations of the measurements, which were taken along the axial height 35 and 125 mm from the inlet.

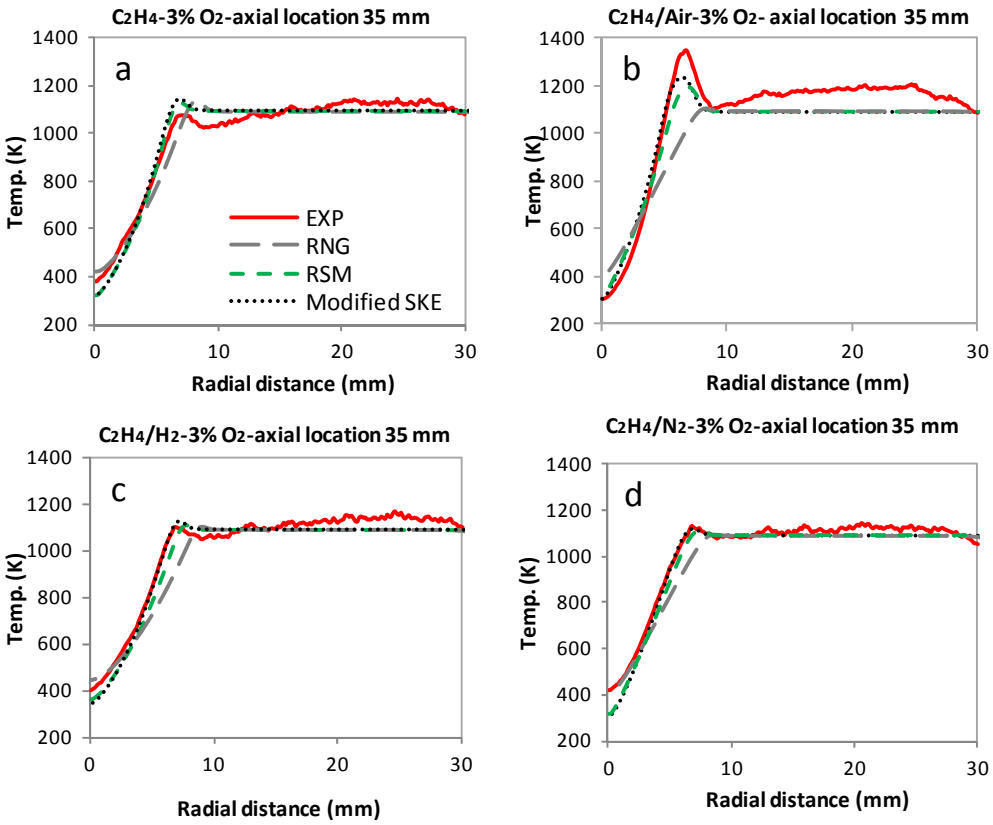

Fig. 4. Effect of turbulence models (modified EDC [15] and GRI-Mech 3.0 mechanism used for the combustion modeling and Discrete Ordinates (DO) model for radiation): comparison between experimental measurement and model predictions at axial location of 35mm for the 3% O_2 coflow oxidant stream and different fuels: (a) C_2H_4, (b) C_2H_4/Air, (c) C_2H_4/H_2, (d) C_2H_4/N_2,

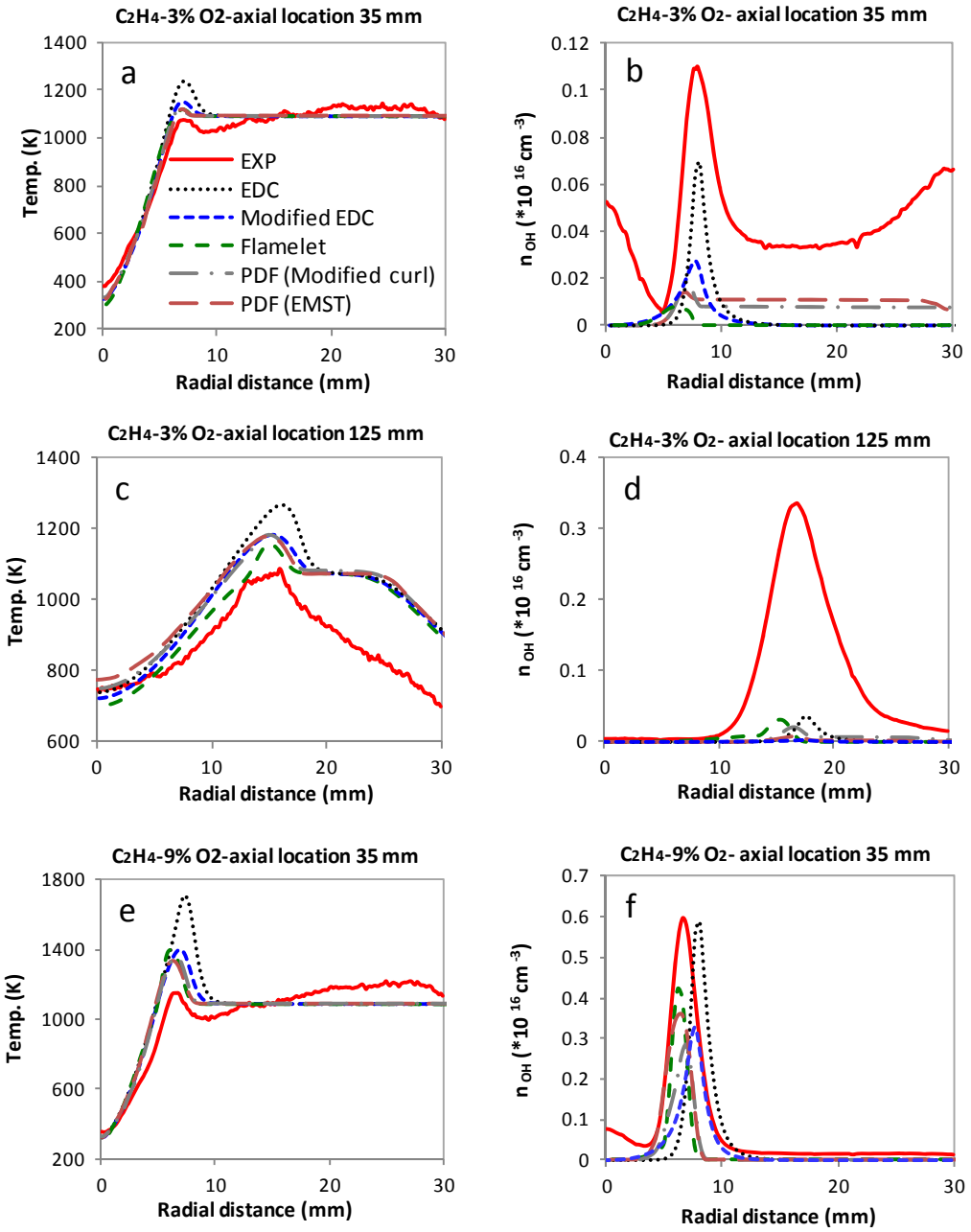

Fig. 5. Effect of turbulent combustion models (adopting the modified SKE turbulence model, GRI-Mech 3.0 mechanism and (DO) radiation model): comparison between experimental measurement [16] and model predictions (temperature (a,c,e) and OH number density (b,d,f)) for 3% O_2 and 9% O_2 ethylene flames

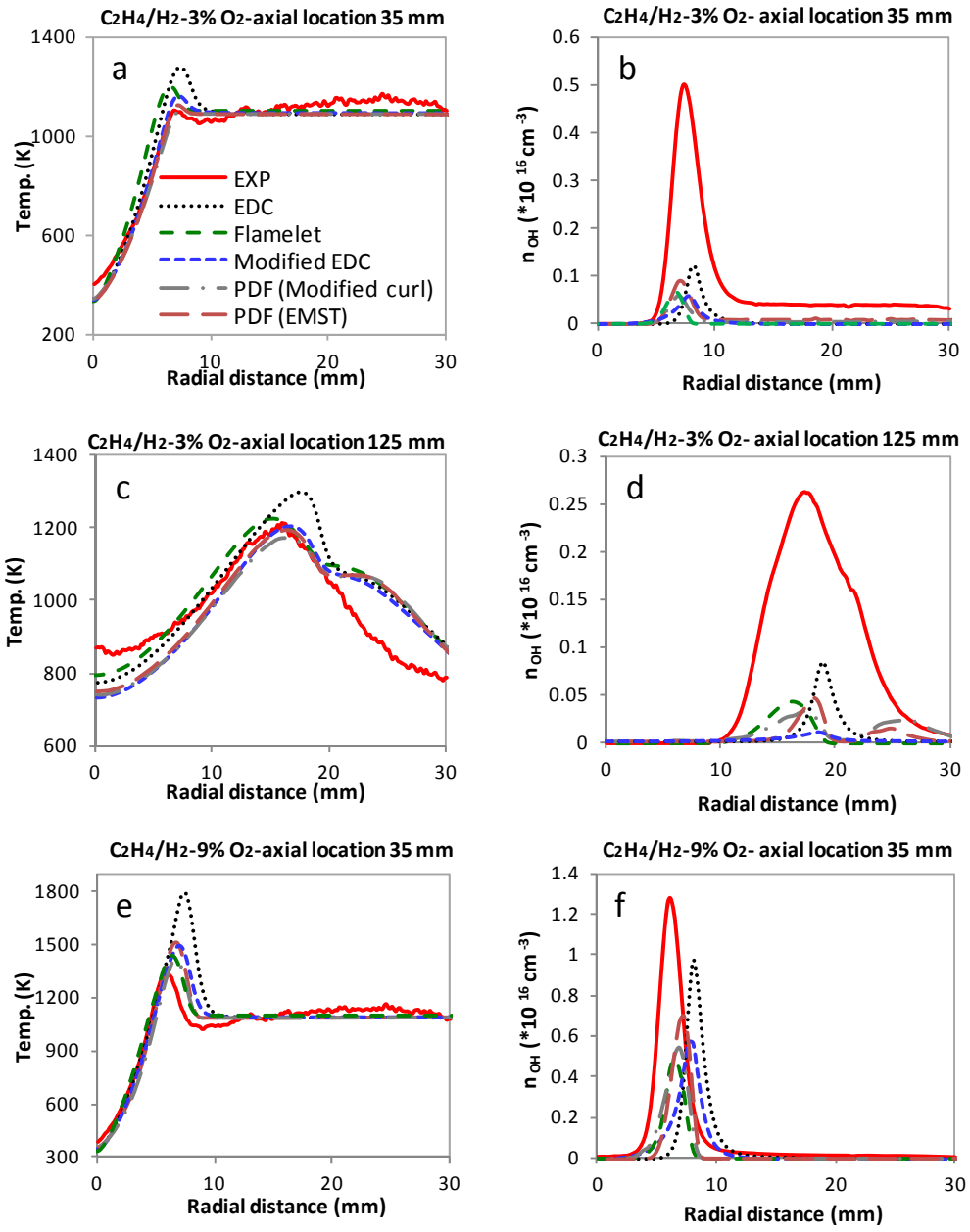

Fig. 6. Effect of turbulent combustion models (adopting the modified SKE turbulence model, GRI-Mech 3.0 mechanism and (DO) radiation model): comparison between experimental measurement [16] and model predictions (temperature (a,c,e) and OH number density (b,d,f)) for 3% O_2 and 9% O_2 ethylene/hydrogen flames.

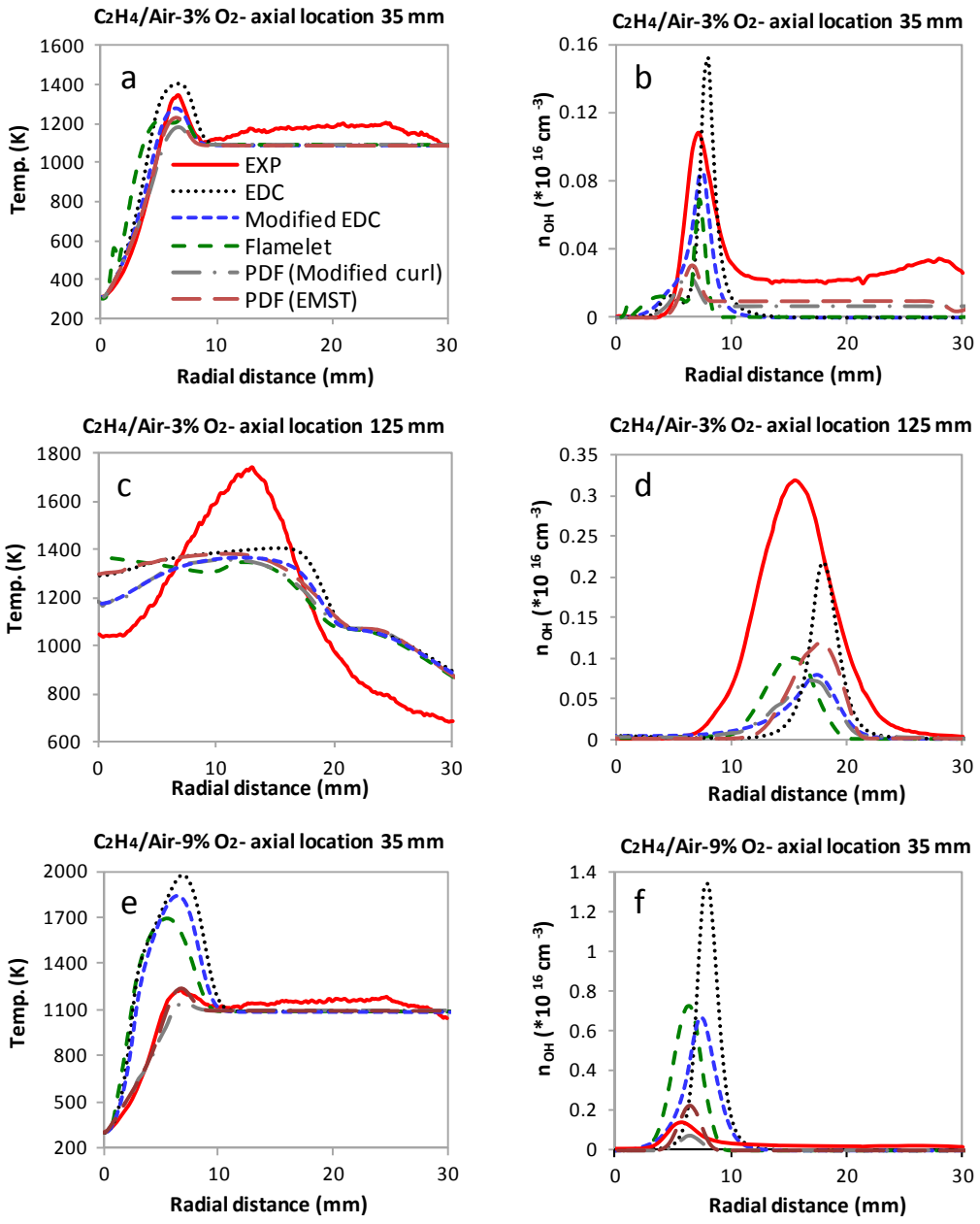

Fig. 7. Effect of turbulent combustion models (adopting the modified SKE turbulence model, GRI-Mech 3.0 mechanism and (DO) radiation model): comparison between experimental measurement [16] and model predictions (temperature (a,c,e) and OH number density (b,d,f)) for 3% O_2 and 9% O_2 ethylene/air flames.

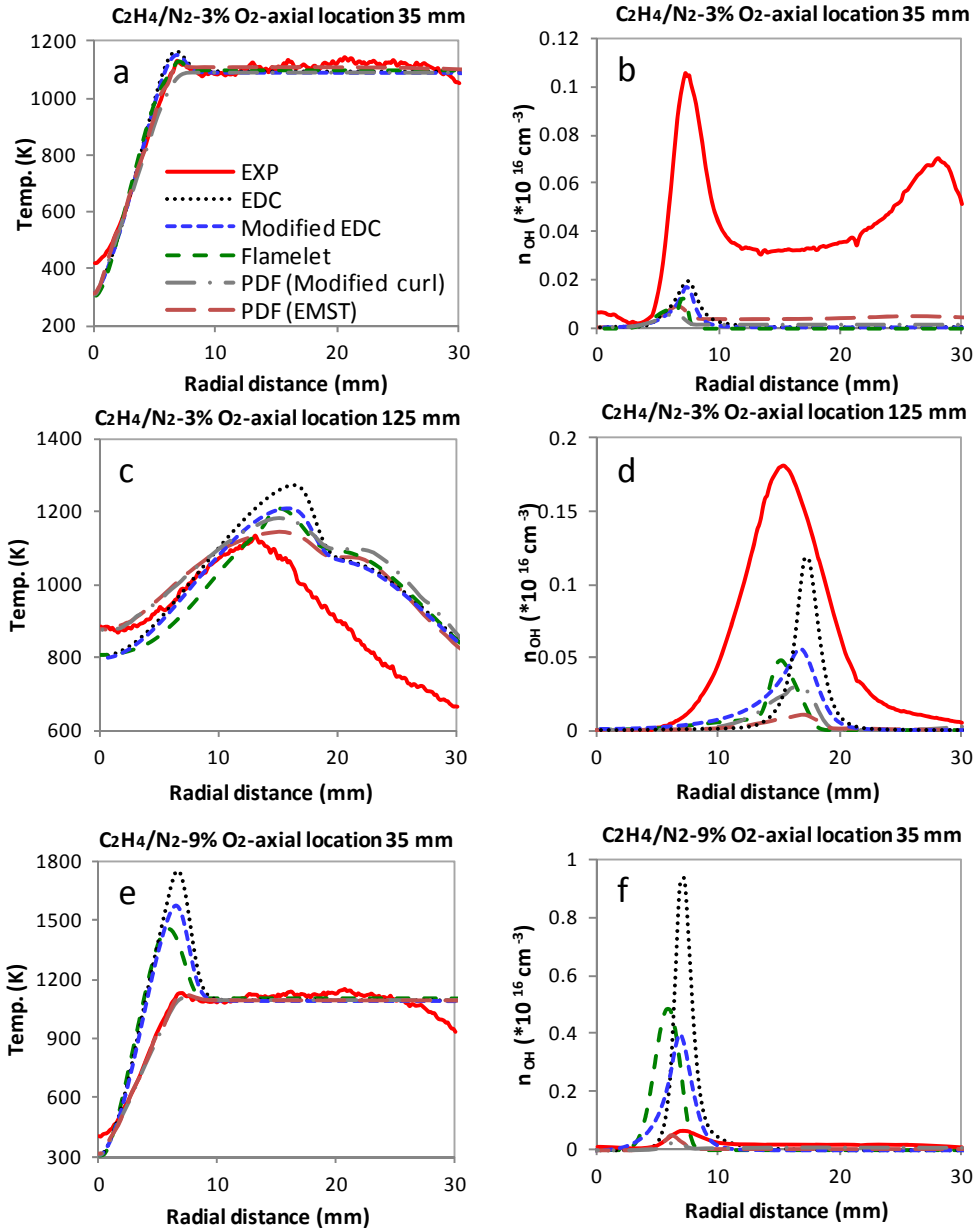

Fig. 8. Effect of turbulent combustion models (adopting the modified SKE turbulence model, GRI-Mech 3.0 mechanism and (DO) radiation model): comparison between experimental measurement [16] and model predictions (temperature (a,c,e) and OH number density (b,d,f)) for 3% O_2 and 9% O_2 ethylene/nitrogen flames.

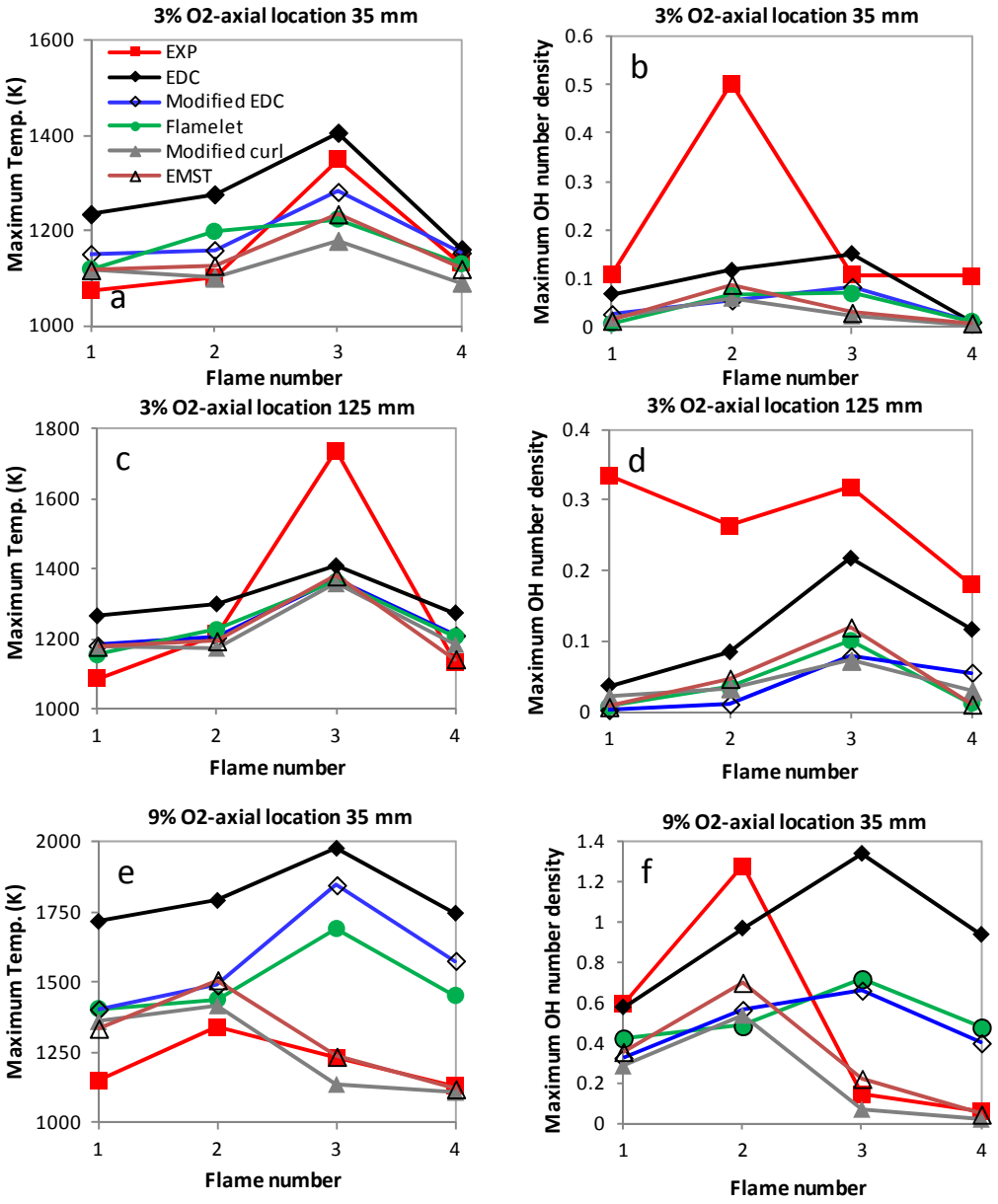

Fig. 9. Maximum temperature and OH number density of experimental measurement [16] and model predictions (different turbulent combustion models) for studied flames. Flame number 1: (C_2H_4), flame number 2: (C_2H_4/H_2), flame number 3: (C_2H_4/air) and flame number 4: (C_2H_4/N_2).

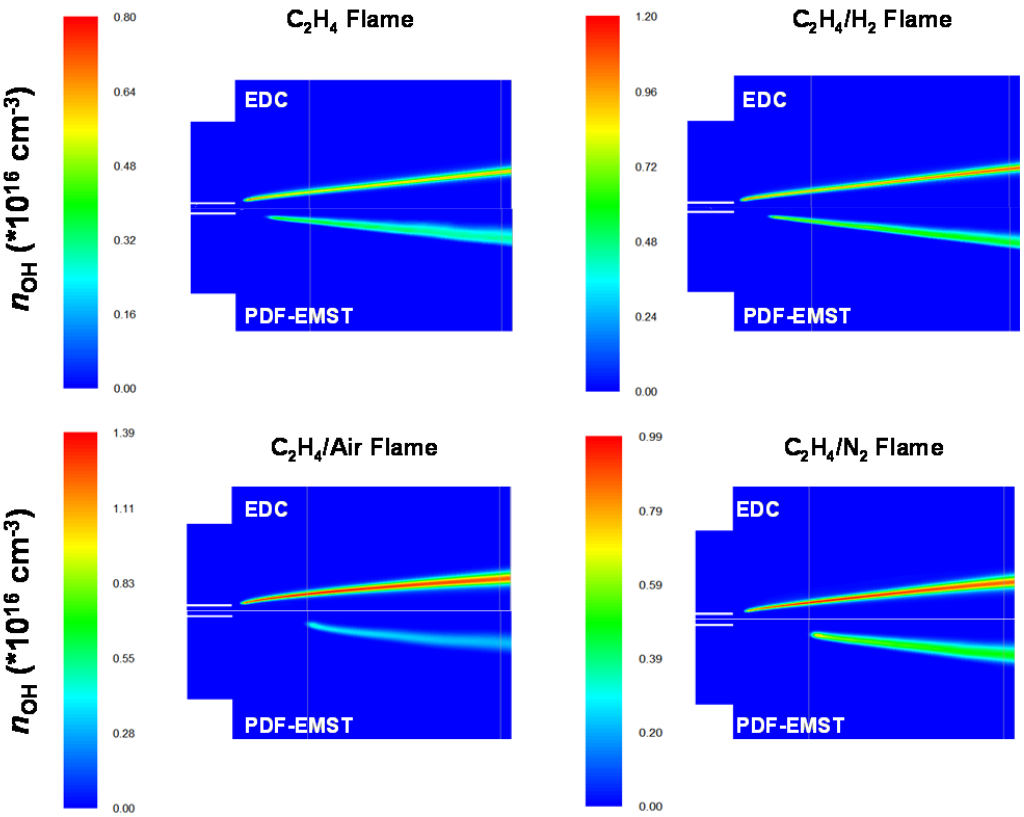

Fig. 10. Predicted OH number densities for the studied flames using the EDC and PDF-EMST models.

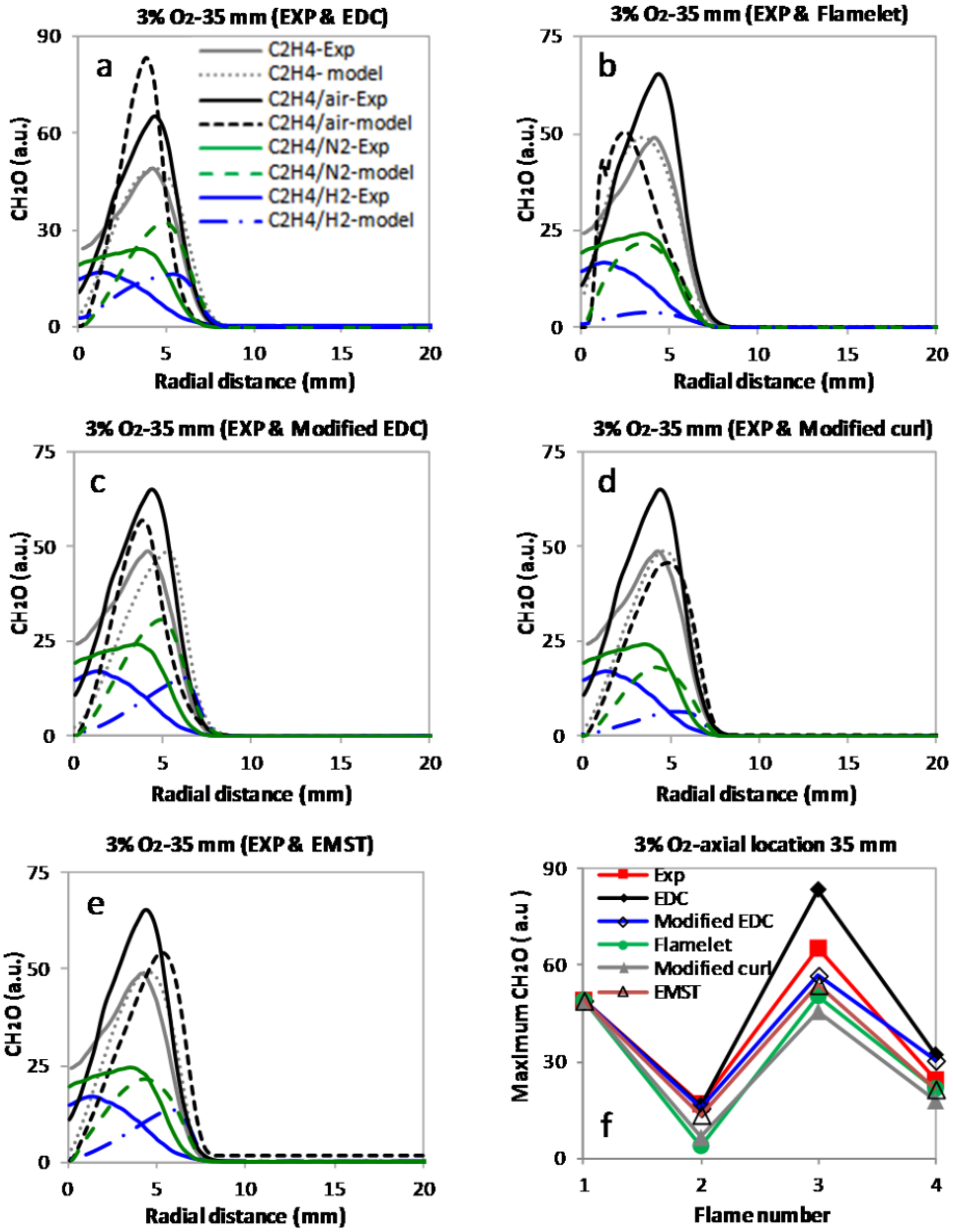

Fig. 11. Experimental [16] and modeling mean radial profile of formaldehyde for 3% flame at axial location of 35mm. Orange: C_2H_4, blue: C_2H_4/H_2, black: C_2H_4/air and green: C_2H_4/N_2. Lines: experimental results and dashed lines: modeling results, (panels a-e).

Panel f: comparison between measured and predicted maximum CH_2O (of panels a-e) using different turbulent combustion models. Flame number 1: (C_2H_4), flame number 2: (C_2H_4/H_2), flame number 3: (C_2H_4/air) and flame number 4: (C_2H_4/N_2).

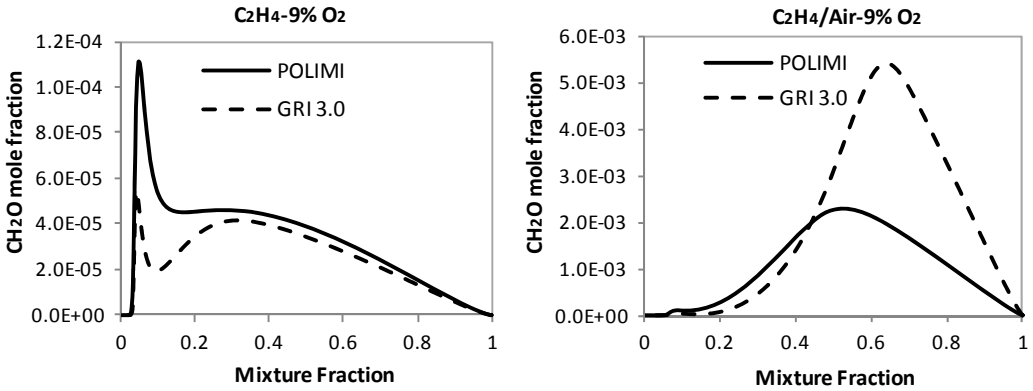

Fig. 12. Comparison between formaldehyde mole fraction of two kinetic mechanisms (GRI 3.0 and POLIMI) found from laminar flame calculation. 9% O_2 coflow oxidant stream. T_{oxi} = 1100 K. $a \approx 200\ s^{-1}$.

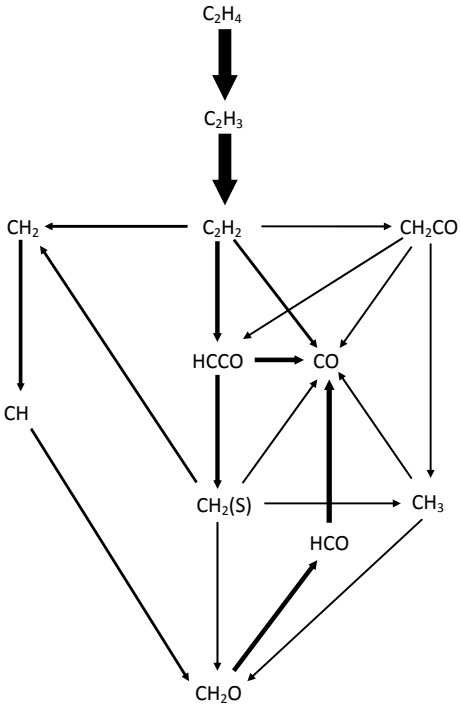

Fig. 13a. Reaction Path Analysis for GRI 3.0 and the conditions of Figure 12a (diffusion flame)

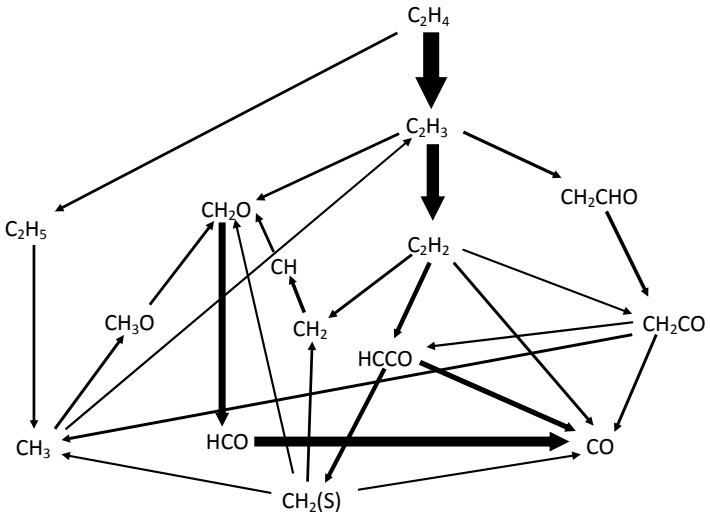

Fig. 13b. Reaction Path Analysis for GRI 3.0 and the conditions of Figure 12b (partially premixed flame)

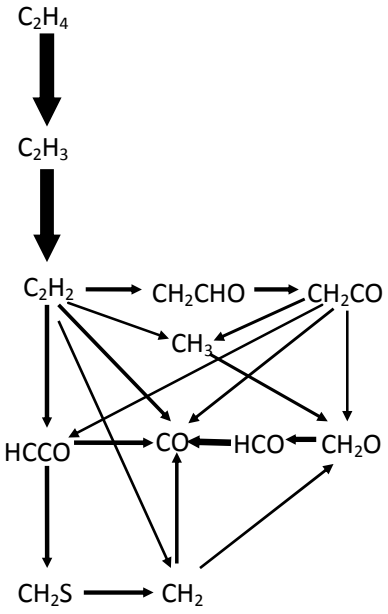

Fig. 14a. Reaction Path Analysis for POLIMI and the conditions of Figure 12a (diffusion flame)

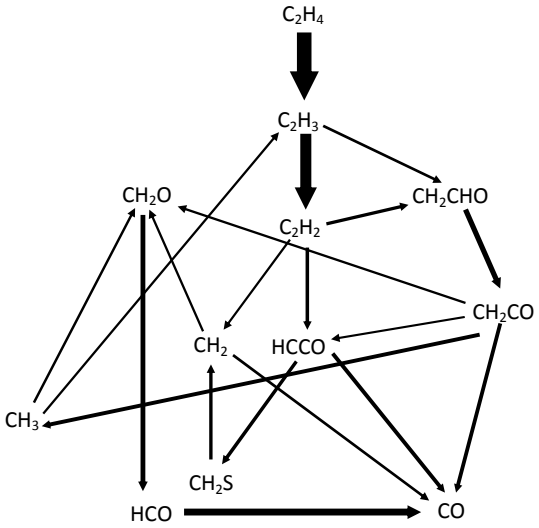

Fig. 14b. Reaction Path Analysis for POLIMI and the conditions of Figure 12b (partially premixed flame)

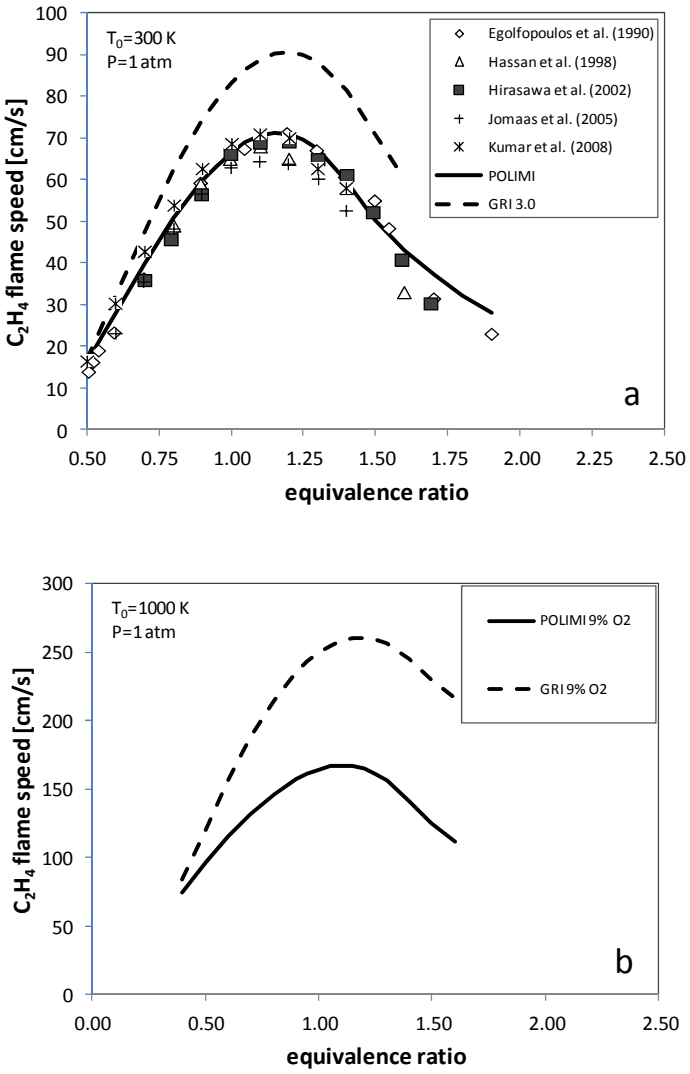

Fig. 15. a. Laminar flame speed of ethylene in air at 1 atm and 300 K. Comparison between GRI 3.0 and POLIMI predicted values with experimental data [46-50], b. Laminar flame speed of ethylene in hot diluted air (9% O_2) at 1 atm and initial temperature of 1000 K. Comparison between GRI 3.0 and POLIMI predicted values.

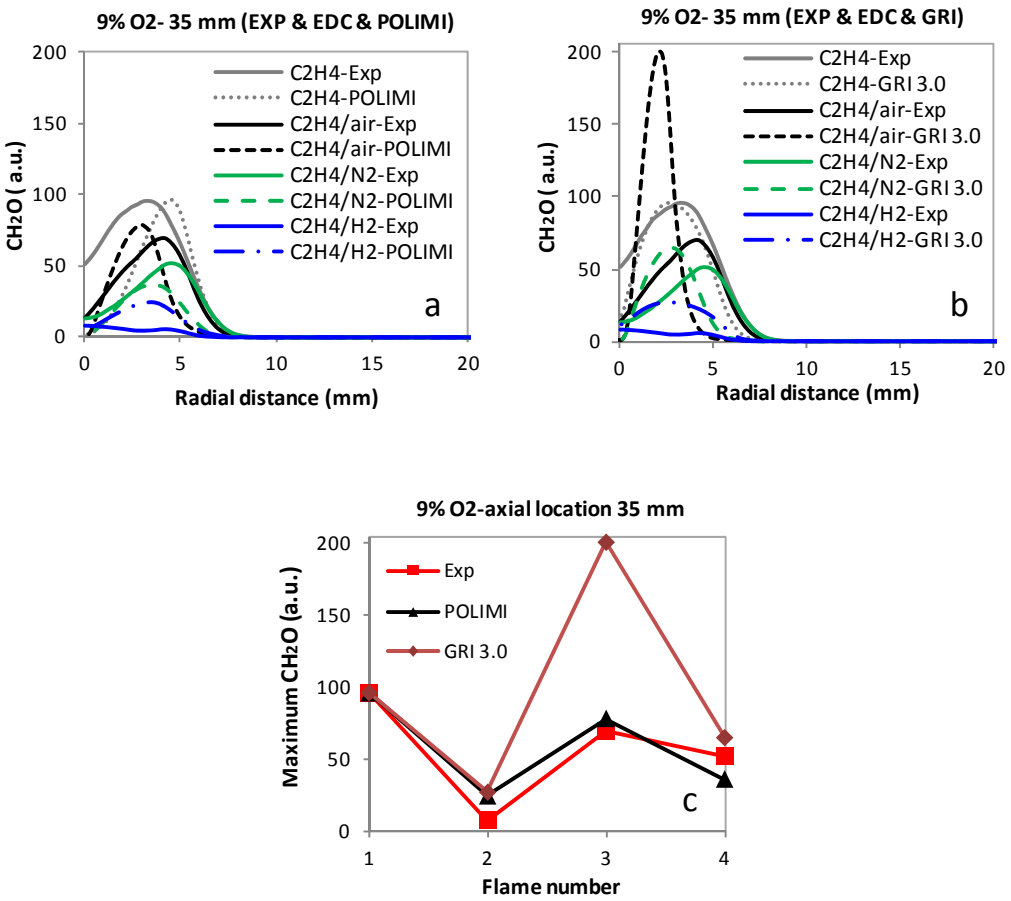

Fig. 16. Experimental and modeling mean radial profile of formaldehyde for 9% flame at axial location of 35mm. Orange: C_2H_4, blue: C_2H_4/H_2, black: C_2H_4/air and green: C_2H_4/N_2. Lines: experimental results and dashed lines: modeling results obtained using the EDC model and two different kinetic mechanisms. (panels a and b). Predicted and measured maximum CH_2O using two kinetic mechanisms. Flame number 1: (C_2H_4), flame number 2: (C_2H_4/H_2), flame number 3: (C_2H_4/air) and flame number 4: (C_2H_4/N_2) (Panel c).

Table 1. Operating conditions of two inlet streams (on a molar basis) for the different case studies.

	Fuel jet						Oxidant flow					
Flame	U(m/s)	T(K)	C_2H_4	H_2	O_2	N_2	U(m/s)	T(K)	O_2	CO_2	H_2O	N_2
C_2H_4-3% O_2	17.5	305	100	0	0	0	2.3	1100	3	3	10	84
C_2H_4-9% O_2	17.5	305	100	0	0	0	2.3	1100	9	3	10	78
C_2H_4/H_2-3% O_2	30.6	305	50	50	0	0	2.3	1100	3	3	10	84
C_2H_4/H_2-9% O_2	30.6	305	50	50	0	0	2.3	1100	9	3	10	78
C_2H_4/air-3% O_2	27.3	305	25	0	15.75	59.25	2.3	1100	3	3	10	84
C_2H_4/air-9% O_2	27.3	305	25	0	15.75	59.25	2.3	1100	9	3	10	78
C_2H_4/N_2-3% O_2	27.3	305	25	0	0	75	2.3	1100	3	3	10	84
C_2H_4/N_2-9% O_2	27.3	305	25	0	0	75	2.3	1100	9	3	10	78

Table 2. Estimated apparent Lift Off (transition points) Error (ELOE) (units: mm) of different turbulent combustion models. The estimate is based on the comparison of predicted and measured temperatures.

	C_2H_4		C_2H_4/H_2		C_2H_4/air		C_2H_4/N_2	
O_2 in coflow	3%	9%	3%	9%	3%	9%	3%	9%
Experiment	-	-	-	-	-	-	-	-
EDC	-25	-30.8	-27.5	-31.1	-9	-30.7	-9	-28.6
Modified EDC	-17	-29	-16	-23	+6	-29.9	-8	-27.6
Flamelet	-18	-28.5	-21	-19	+9	-33	-5	-30.8
PDF transport (Modified curl)	-8	-19.5	-4	-12	+6	+4	+3	-1
PDF transport (EMST)	-7	-18.5	-5	-15	+5	0	-2	-0.9

Kinetic and fluid dynamic modeling of ethylene jet flames in diluted and heated oxidant stream combustion conditions

Seyed Reza Shabanian[1,3], Paul Ross Medwell[2], Masoud Rahimi[*,1], Alessio Frassoldati[**,3], Alberto Cuoci[3]

*masoudrahimi@yahoo.com; **alessio.frassoldati@polimi.it

1-CFD Research Center, Chemical Engineering Department, Razi University, Kermanshah, Iran

2-School of Mechanical Engineering, The University of Adelaide, South Australia 5005, Australia

3-Politecnico di Milano, Dipartimento di Chimica, Materiali e Ingegneria Chimica "G. Natta", Milano, Italy

Supplemental Material

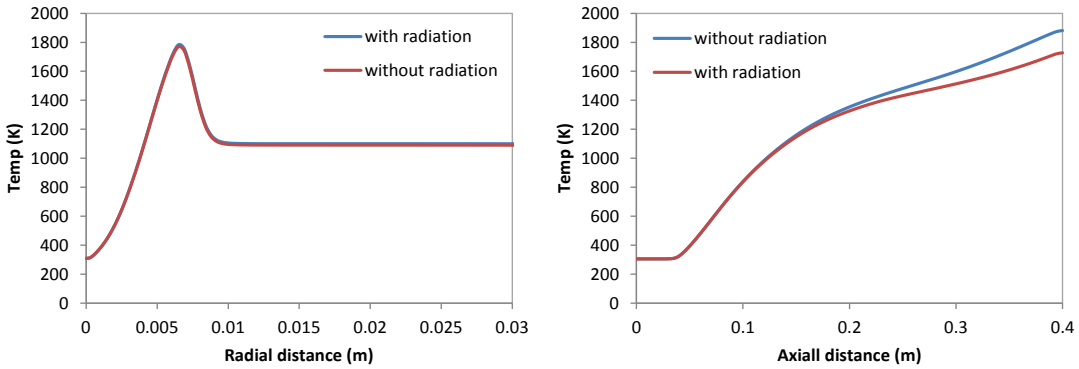

Figure S1. Effect of radiation model (Discrete Ordinates) for the C_2H_4/N_2 flame with 9% O_2 in the coflow.

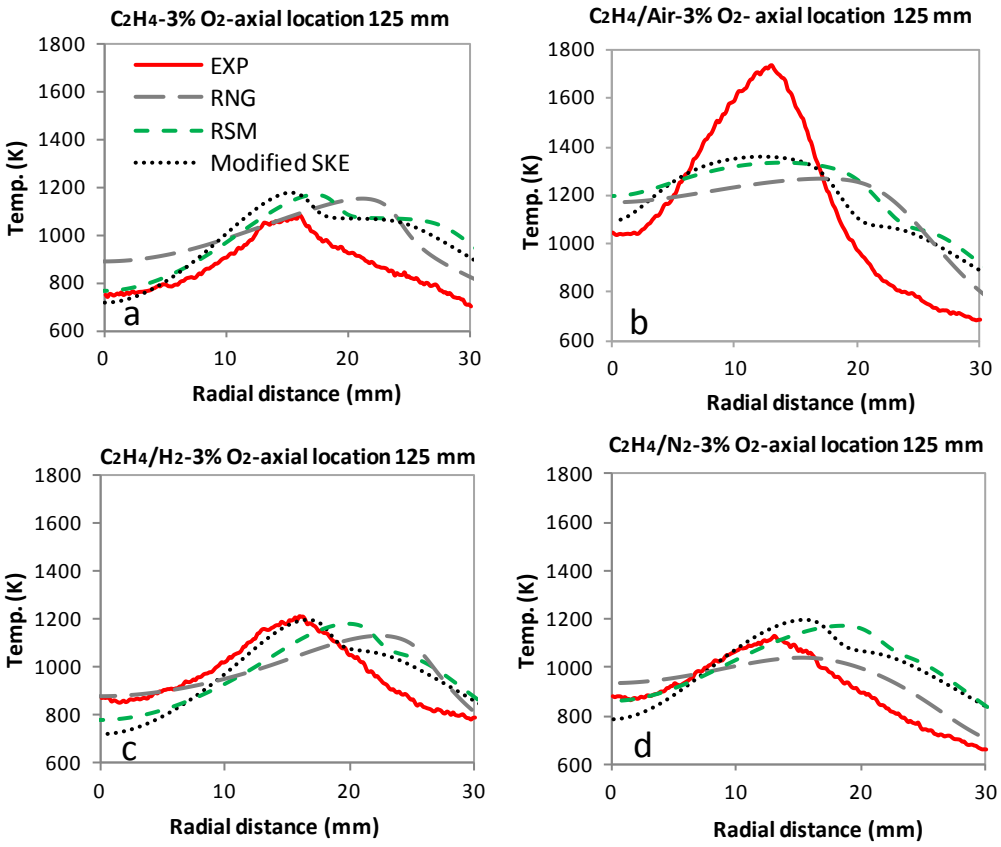

Figure S2. Effect of turbulence models (modified EDC [15] and GRI-Mech 3.0 mechanism used for the combustion modeling and Discrete Ordinates (DO) model for radiation): comparison between experimental measurement [16] and model predictions at axial location of 125mm for the 3% O_2 coflow oxidant stream and different fuels: (a) C_2H_4, (b) C_2H_4/Air, (c) C_2H_4/H_2, (d) C_2H_4/N_2.

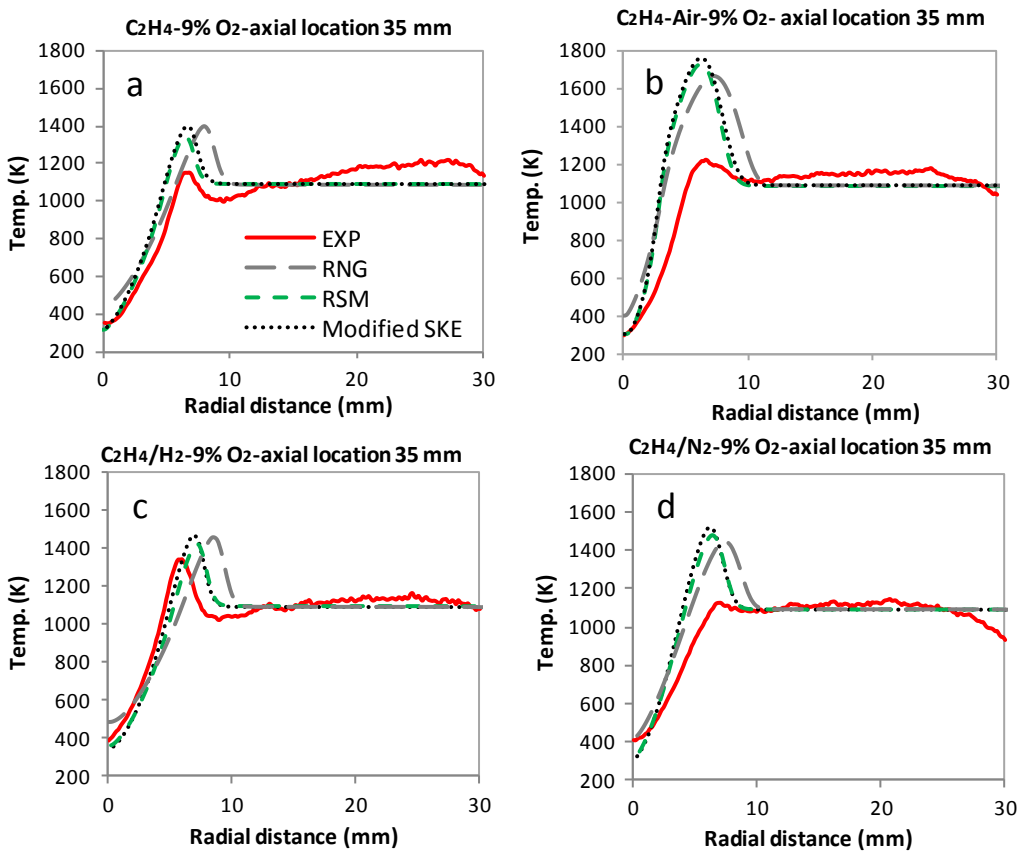

Figure S3. Effect of turbulence models (modified EDC [15] and GRI-Mech 3.0 mechanism used for the combustion modeling and Discrete Ordinates (DO) model for radiation): comparison between experimental measurement [16] and model predictions at axial location of 35mm for the 9% O_2 coflow oxidant stream and different fuels: (a) C_2H_4, (b) C_2H_4/Air, (c) C_2H_4/H_2, (d) C_2H_4/N_2.

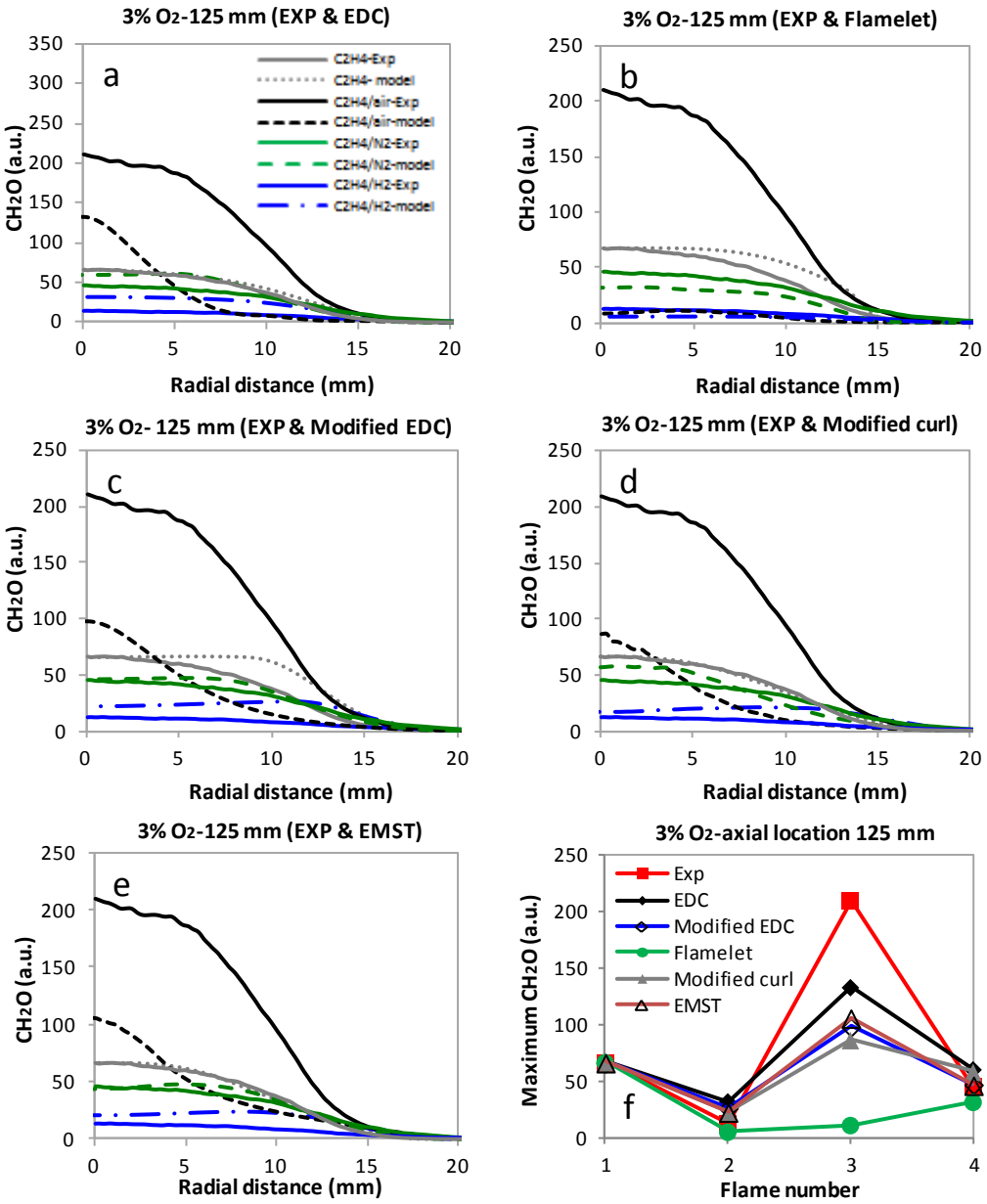

Figure S4. Experimental and modeling mean radial profile of formaldehyde for 3% flame at axial location of 125mm. Orange: C_2H_4, blue: C_2H_4/H_2, black: C_2H_4/air and green: C_2H_4/N_2. Lines: experimental results and dashed lines: modeling results, (panels a-e).

Panel f: comparison between measured and predicted maximum CH_2O (of panels a-e) using different turbulent combustion models. Flame number 1: (C_2H_4), flame number 2: (C_2H_4/H_2), flame number 3: (C_2H_4/air) and flame number 4: (C_2H_4/N_2).

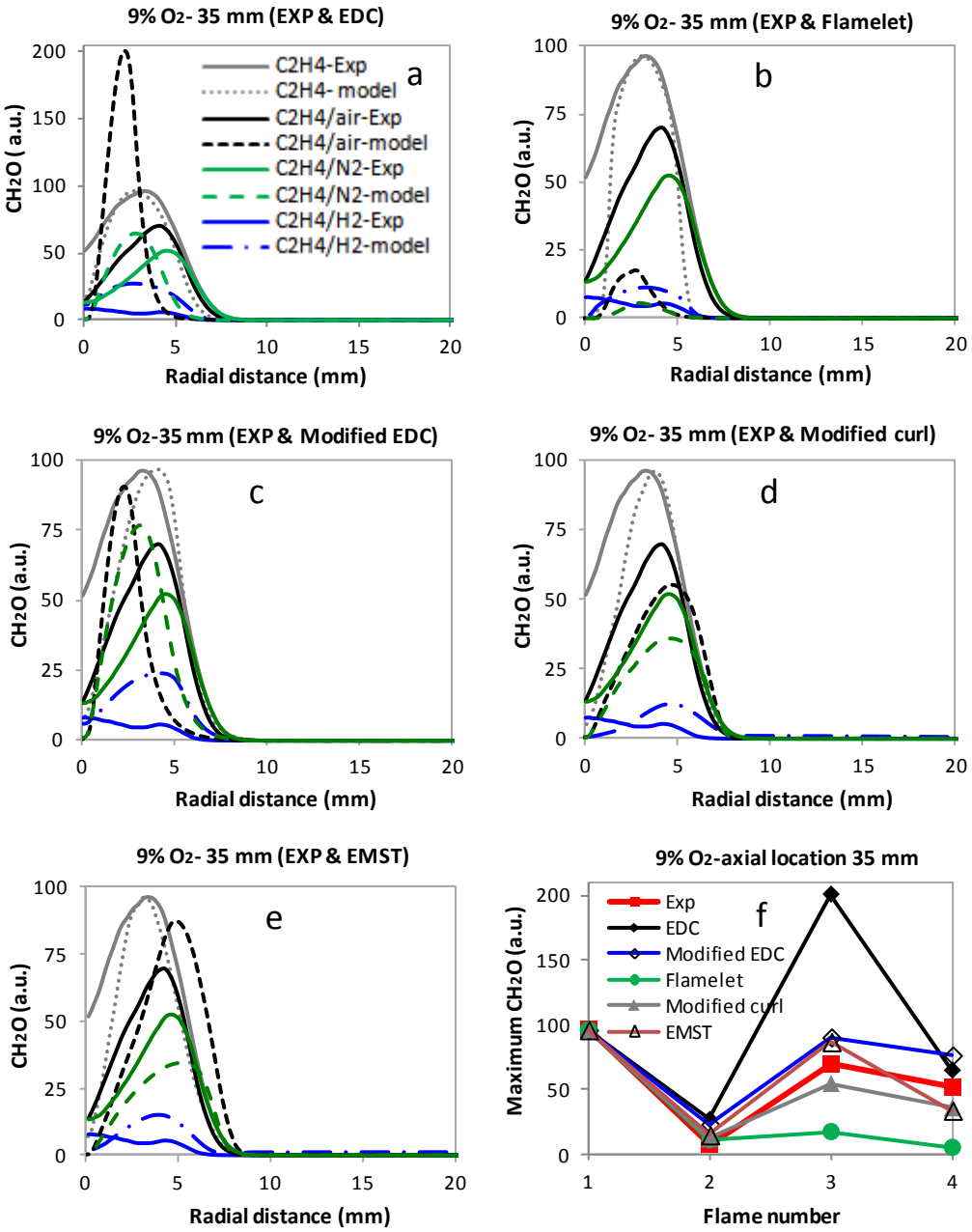

Figure S5. Experimental and modeling mean radial profile of formaldehyde for 9% flame at axial location of 35mm. Orange: C_2H_4, blue: C_2H_4/H_2, black: C_2H_4/air and green: C_2H_4/N_2. Lines: experimental results and dashed lines: modeling results, (panels a-e).

Panel f: comparison between measured and predicted maximum CH_2O (of panels a-e) using different turbulent combustion models. Flame number 1: (C_2H_4), flame number 2: (C_2H_4/H_2), flame number 3: (C_2H_4/air) and flame number 4: (C_2H_4/N_2).

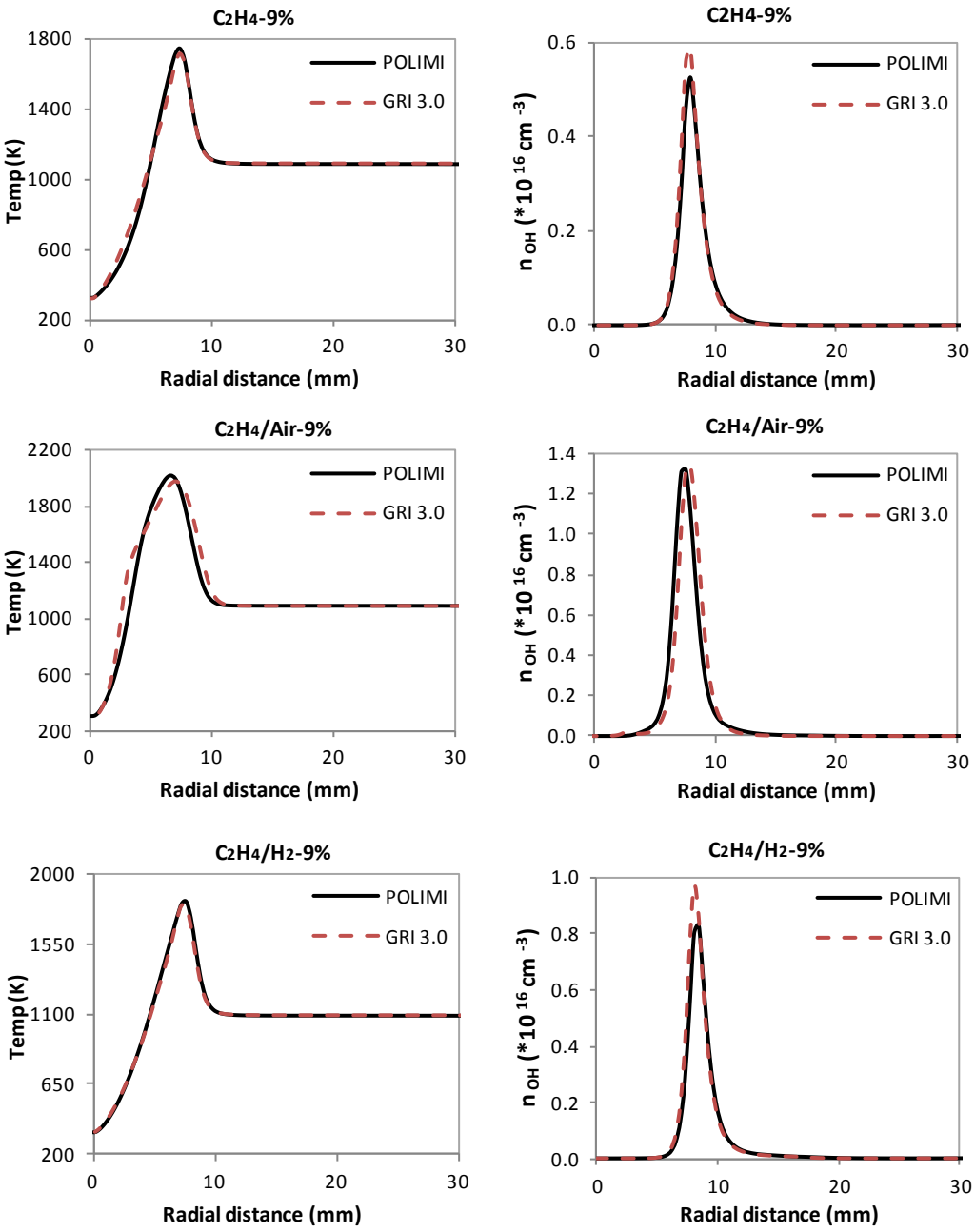

Figure S6. Predicted radial profiles of temperature and OH number density at an axial location of 35mm. Red lines: GRI-Mech 3.0 mechanism. Black lines: POLIMI mechanism.